

# Mesoscale modelling in China: Risø DTU numerical wind atlas calculation for NE China (Dongbei)

**Badger, Jake; Larsén, Xiaoli Guo; Hahmann, Andrea N.; Rong, Zhu; Chunhong, Yuan**

*Publication date:*
2010

*Document Version*
Publisher's PDF, also known as Version of record

# Mesoscale modelling in China: Risø DTU numerical wind atlas calculation for NE China (Dongbei)

Risø-I-Report

Jake Badger, Xiaoli Guo Larsén, Andrea Hahmann, Zhu Rong, Yuan Chunhong
Risø-I-3070(EN)
June 2010

Risø DTU
National Laboratory for Sustainable Energy

**Author:** Jake Badger, Xiaoli Guo Larsén, Andrea Hahmann, Zhu Rong, Yuan Chunhong
**Title:** Mesoscale modelling in China: Risø DTU numerical wind atlas calculation for NE China (Dongbei)
**Division**: Wind Energy Division

**Risø-I-3070(EN)**
**June 2010**

**Abstract (max. 2000 char.):**

This document reports on the methods and findings of project "A01 Mesoscale Modelling", part of the CMA component of the Wind Energy Development (WED) programme, focusing mainly on the methods and work undertaken by Risø DTU. The KAMM/WAsP methodology for numerical wind atlas calculation of the wind resource for Dongbei south of 50°N. The results of the numerical wind atlas show a wind resource over the region of interest modulated mainly by topographic features. These are principally elevated terrain features, giving high resources on exposed ridges and lower resources adjacent to the low slopes of mountains and large-scale valley features. A comprehensive verification was carried in which the generalized wind climates derived from mesoscale modelling and measurements for nine meteorological stations were compared. A mean absolute error of 8 % for 50 m wind speeds was determined. The major new aspects of the project were the large number of KAMM/WAsP sensitivity studies, comparison with WRF, and the CMA's numerical wind atlas method (WERAS). Additionally, the reliability of the input data for the methodology, and the wave-number spectra properties of the output data were investigated. Comparison and verification of the results of CMA's numerical wind atlas method (WERAS) were carried out. Generalized wind climates show a positive bias compares to measurement, though an improved generalization method is thought will improve this result. A more direct comparison was made between KAMM and WRF by using KAMM wind classes in WRF, run in idealized mode. A smoother resource map was given by WRF and different gap flow behaviour was noted. Future work would be well directed towards i. improving the method for importing WRF results into WAsP, ii. developing relationships between the sensitivity analysis and uncertainties, iii. continuing the measurements at current sites and additional sites, in order to improve and enhance the verification analysis.

**Contract no.:**

**Groups own reg. no.:**
1170040-01

**Sponsorship:**
Danida

**Cover:**

**Pages: 69**
**Tables: 6**
**References: 10**

Information Service Department
Risø National Laboratory for Sustainable Energy
Technical University of Denmark
P.O.Box 49
DK-4000 Roskilde
Denmark
Telephone +45 46774005
bibl@risoe.dtu.dk
Fax +45 46774013
www.risoe.dtu.dk

# Contents

# 1 Summary

This document reports on the methods and findings of project "A01 Mesoscale Modelling", part of the CMA component of the Wind Energy Development (WED) programme. This report focuses on the methods and work undertaken by Risø DTU. Another report written by CMA will focus on the methods and work undertaken by CMA.

Risø DTU has employed the KAMM/WAsP methodology for numerical wind atlas calculation of the wind resource for Dongbei south of 50$^{o}$N. The three north-eastern provinces of China cover a large area which needed to be broken down into three modelling domains. The KAMM/WAsP method is built upon a statistical–dynamical downscaling methodology in which wind classes are defined to represent the range of large-scale atmospheric climate conditions. Each of the three modelling domains has its own sets of wind classes, as the large-scale meteorological conditions change over the region of interest. The results of the numerical wind atlas show a wind resource over the region of interest modulated mainly by topographic features. These are principally elevated terrain features, giving high resources on exposed ridges and lower resources adjacent to the low slopes of mountains and large-scale valley features. In the flat plain regions of the provinces the wind resource is fairly uniform, due to the uniformity of wind speed forcing by the large-scale wind climate. A comprehensive verification was carried in which the generalized wind climates derived from mesoscale modelling and measurements for nine meteorological stations were compared. A mean absolute error of 8% for 50 m wind speeds was determined.

The major new aspects of the project were the large number of KAMM/WAsP sensitivity studies, comparison with WRF, and the CMA's numerical wind atlas method (WERAS). Additionally, the reliability of the input data for the methodology, and the wave-number spectra properties of the output data were investigated. All these studies were carried out to assess the contribution of each step in the methodology to uncertainty in the resources. Comparison and verification of the results of CMA's numerical wind atlas method (WERAS) were carried out. The simulated wind resources from WERAS give similar results, though somewhat smoother, compared to KAMM/WAsP. However, generalized wind climates show a positive bias compares to measurement. Further development of the generalization method is thought will improve this result. A more direct comparison was made between KAMM and WRF by using KAMM wind classes in WRF, run in idealized mode. Again a smoother resource map was given by WRF and different gap flow behaviour was noted.

Future work would be well directed towards i. improving the method for importing WRF results into WAsP, ii. developing relationships between the sensitivity analysis and uncertainties, iii. continuing the measurements at current sites and additional sites, in order to improve and enhance the verification analysis.

# 2 Introduction

The main objects of the "A01 Mesoscale modelling" project were

- to calculate the numerical wind atlas for the three north-eastern provinces of China (Dongbei region)
- to verifiy the numerical wind atlas against measurements made in the project "A02 Measurements" and analysised in the project "A03 Microscale modelling"
- to expand CMA's and Risø-DTU's experience within numerical wind atlas methodologies, across a range of mesoscale models, and across a range of pre-processing and post-processing techniques, through scientific collaboration
- to identify areas for research and development for numerical wind atlas methods in Dongbei

This report describes how the work towards the fulfilment of these objects was carried out. First, a description of the current method for numerical wind atlas calculations is given and the results presented, in Sections 3, 4, and 5. Then, in Section 6, 7, 8, 9, and 10, the issue of wind resource error and uncertainty is addressed. This is done by examining the steps of the methodology in detail and investigating sensitivity of the modelling results to alterations in the set-up. In Section 11 verification of the numerical wind atlas results is carried out using the measurement results from Mortensen et al (2010). In Section 12, an indexing of the mesoscale topography is presented, relating to the uncertainty of the wind resource results. In Section 13, comparison and verification of CMA's WERAS method are presented. Wave-number spectral analyses of the KAMM/WAsP and CMA's WERAS wind resource maps are given in Section 14. In Section 15, a comparison of KAMM and WRF, this time run in idealized mode, is presented. Section 16 outlines the main conclusions of the project. Sections 19 and 20 provide appendices for placement of extra figures and data file descriptions.

# 3 Description of Method

## 3.1 General description

The conventional method used to produce estimates of wind resource large regional scales is to analyse wind measurements made at a number of sites around the region in question, as in for example the European Wind Atlas (Troen and Petersen, 1989). In order for this method to work there needs to be a sufficient quantity of high quality data, covering the entire region. This criterion is sometimes difficult to satisfy and therefore other methods are required – methods that will not meet bankable accuracy in resource estimates, but on the other hand that will typically give good indications of the geographical distribution of the wind resource and that will be very useful for decision making and planning of feasibility studies and of actual project preparation.

Numerical wind atlas methodologies have been devised to solve the issue of insufficient wind measurements. One such methodology is the KAMM/WAsP method developed at Risø National Laboratory (Frank and Landberg, 1997).

In this methodology an approach called statistical-dynamical downscaling is used (Frey-Buness et al, 1995). The basis for the method is that there is a robust relationship between meteorological situations at the large-scale and meteorological situations at the small-scale.

Information about the large-scale meteorological situation is freely available from the NCEP/NCAR reanalysis data-set. This data-set has been created by assimilating measurement data from around the globe in a consistent fashion from 1948 to the present day. The primary purpose for the generation of this data-set is to provide a reference for the state of the atmosphere and to identify any features of climate change. Another application of the data-set is as a long term record of large-scale wind conditions. The NCEP/NCAR data is used to create around 100 to 150 different large-scale wind situations, called wind classes that represent the large-scale wind climate.

In order to make these wind classes meaningful at a smaller scale a mesoscale model is used to find out how the large-scale wind forcing is modified by regional scale topography. Therefore for each wind class a mesoscale model simulation is performed using the Karlsruhe Atmospheric Mesoscale Model (KAMM, Adrian and Fiedler, 1991).

Post-processing of the results from all the simulations yields a wind resource map at the resolution of the model simulations. Further analysis of the results from the simulations with consideration to the topography as described in the mesoscale model, yields wind atlas maps for generalized surface conditions. Files containing detailed information about the wind speed and direction distributions can also be generated that are directly compatible with the WAsP software, the wind industry standard for site resource assessment calculations.

## 3.2 Mesoscale models

The Karlsruhe Atmospheric Mesoscale Model (KAMM) is a 3D, non-hydrostatic, and incompressible mesoscale model. It is described in Adrian and Fiedler (1991), and Adrian (1994). Spatial derivatives are calculated in the model by central differences on a terrain following grid. The turbulent fluxes are modelled using a mixing-length model with stability dependent turbulent diffusion coefficients in stably stratified flow, and a non-local closure for the convective mixed layer. Lateral boundary conditions assume zero gradients normal to the inflow sides. On outflow boundaries, the horizontal equations of motion are replaced by a simple wave equation allowing signals to propagate out of the domain without reflection. Gravity waves can penetrate the upper boundary outward using the boundary condition of Klemp and Durran (1983).

KAMM is able to run as a "stand-alone" model, i.e. the model can be run by using only the large scale forcing in the form of a single vertical profile of geostrophic wind and virtual potential temperature. Hence, it is not necessary to nest the mesoscale model within larger model that must supply the boundary conditions. At regional scales the mesoscale model is used to model atmospheric flows in domains of order 500km x 500km x 5km.

## 3.3 Topographic data

Data concerning the surface elevation comes from the SRTM30 dataset. The dataset can be accessed via ftp://e0mss21u.ecs.nasa.gov/srtm/srtm30. This data uses a longitude-latitude projection at 30 arc second resolution. This elevation data is manipulated first to change it to a UTM coordinate system and then to change the resolution appropriately for the mesoscale simulations.

Data concerning the surface roughness is derived from the United States Geological Survey (USGS) Global Land Cover Classification, also known as GLCC. The data can be accessed via http://edcsns17.cr.usgs.gov/glcc/. This data is given using the Lambert azimuthal projection. This land cover data is converted to UTM coordinate system and then to the appropriate resolution. It is also converted from land cover data to surface roughness data. This is done by using a look-up table that relates specific land cover classifications to specific surface roughness.

## 3.4 Meteorological data

Atmospheric data is obtained from the NCEP/NCAR reanalysis data-set (Kalnay, 1996). Data is given on a longitude-latitude grid with a resolution of 2.5 x 2.5 degrees at 1000, 850, 700 and 500 hPa isobaric surfaces. This data needs to be converted into geostrophic wind and potential temperature values for different heights in meters in the atmosphere. The data is compiled into long time series data for use in the wind class generation programs. The Climate Diagnostics Centre provides access to the NCEP/NCAR reanalysis via http://www.cdc.noaa.gov/cdc/reanalysis/. The NCEP/NCAR data from 1977 to 2008 has been used for the numerical wind atlas studies described in this chapter.

## 3.5 Modelling domains

Creating a numerical wind atlas demands a large computational effort, and this computation effort increases with the size of the region to be mapped. The Dongbei provinces' large size means that it is not possible to perform the numerical wind atlas calculations for the whole region using one calculation domain. Therefore it was decided to split the numerical wind atlas effort into three calculation domains. The domains used

for numerical wind atlas calculation are shown in Figure 1. The bounds of the domains are given in Table 1.

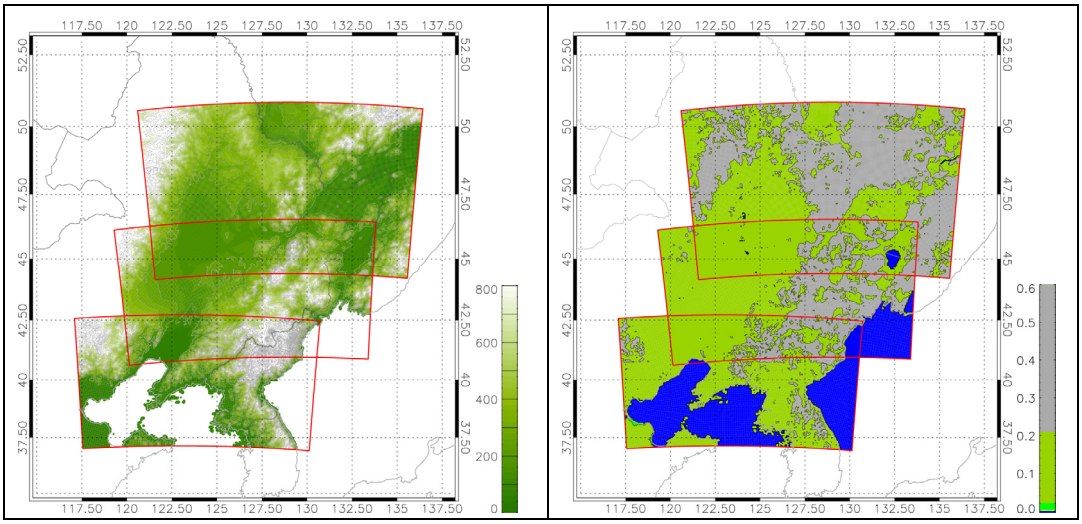


*Figure 1: Map of the calculation domains showing the orography (left) and surface roughness lengths (right). The domains are shown by the red outlined rectangles. The domains are defined in UTM coordinates. Colour bars give the elevation and roughness length in metres. Note the highest elevations exceed 800 m.*

*Table 1: The bounds of the three modelling domains in UTM coordinates. The number of size of the grid at 5 km resolution is given by nx and ny in the table.*

| Domain name | Min x [km] | Max x [km] | Min y [km] | Max y [km] | UTM zone | Datum | nx | ny |
|---|---|---|---|---|---|---|---|---|
| NN northern domain | -95 | 1025 | 4915 | 5635 | 52 | WGS84 | 225 | 145 |
| NC centre domain | -250 | 870 | 4535 | 5155 | 52 | WGS84 | 225 | 125 |
| NS southern domain | 15 | 1135 | 4110 | 4730 | 51 | WGS84 | 225 | 125 |

# 4 Wind classification system

The time series data of wind and temperature profiles derived from NCEP/NCAR reanalysis data is used to determine approximately 100 to 150 wind classes. These wind classes form a representative set of wind conditions for the region. The wind classes represent different wind speed, wind directions, atmospheric stability or shear.

A way to measure the likely impact of an obstacle, such as a hill, on a flow is to calculate the Froude number. The Froude Number is U / (h * N), where U = velocity scale, h = height scale of obstacle, N = Brunt-Väisälä frequency, where $N^2 = g/\theta_0(d\theta/dz)$. For cases where the Froude number is below one, the flow tends to flow around obstacles. For cases where the Froude number is above one, the flow tends to over obstacles. More stable conditions tend to lead to lower Froude number flow behaviour, in which channelling between or around obstacles is more prevalent, as well as lee effects to be more persistent. The figures of the example simulated wind fields that follow for the different computational domains, also show examples of different Froude number flow for similar wind speeds.

The inverse Froude number squared is used in the wind class classification system to differentiate meteorological situations that have similar wind speed and direction but different thermal stratification. The height scale used is 1500 m, which is the height difference between the first and second level in the wind class profile.

Wind classes are defined by first splitting the reanalysis profile data into twelve equal size direction sectors according to the geostrophic wind at 0 m (note: 1500 m is also used in Section 9.2). Then, for each direction sector, the data is divided into a number of wind speed bins. Some of these wind speed bins are further split into stability classes according to Froude number; for example, if two stability classes are used the dividing line is the median value of Froude number for the wind speed bin in question. A maximum number of wind-speed-Froude-number bins can be prescribed also. The actual number of wind classes per sector is determined by the setting of the minimum frequency allowed for a wind class. The wind speed bin limits are defined such that wind-speed-Froude-number frequencies within a sector are equal, except for the lowest and highest wind speed bins which have a lower frequency in order to better represent the tails of the wind speed distribution.

An advantageous feature of the wind class method is that the frequency of occurrence of the wind classes can be recalculated for different periods. When the wind classes are defined, a 30-year period is used to evaluate the wind class frequencies. However, as is often the case, the period over which measurements are available may be significantly less. In this study, 2009 is defined at the measurement period. So the appropriate value of the wind classes is obtained by recalculating the wind classes frequencies using the only the reanalysis data for 2009.

Figure 2 gives the wind classes sets for the three modelling domains. There are 137, 124, 128 wind classes for the NN, NC, and NS domains, respectively. The wind classes are plotted by using a diagram using a polar coordinate. Each cross represents a wind class. The location of the cross indicates the wind vector of that wind class. The distance from

the centre gives the wind speed and the angle gives the wind directions. The size of the cross indicates the frequency of occurrence, the larger the cross the more frequently the wind class occurs. A scale relating the wind class frequency with the size of the crosses is given in each figure. The colour of the crosses indicates the stability of the wind class, as given by the Froude number. The Froude number is used to distinguish wind classes with similar wind speed and direction but different stability condition, as described earlier in this chapter. By convention the plot actually is giving the reciprocal or inverse of the Froude number. A colour scale is given in each figure relating the colour of the crosses to inverse Froude number values.

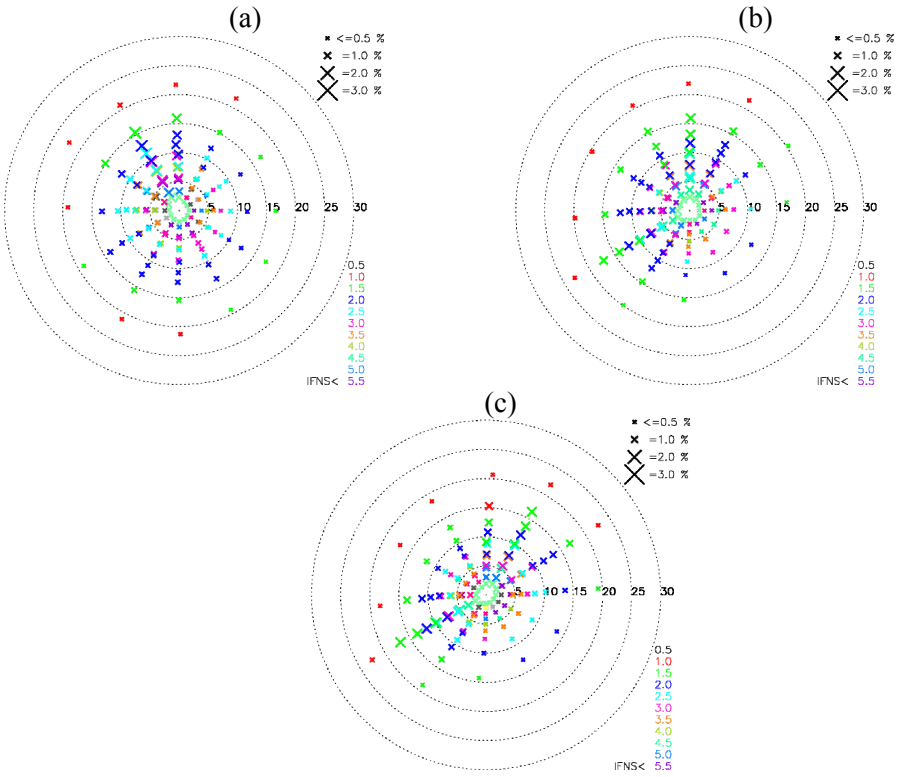


*Figure 2: Plots showing the wind class sets for the 3 domains, (a) northern domain set defined at 126.25E 48.75N, (b) centre domain set defined at 123.75E 43.75N and (c) southern domain set defined at 121.25E 41.25N. Each cross represents a forcing wind speed (distance from the centre of the diagram) and direction. The speed scale is in m/s. The colours indicate the inverse Froude number squared (IFNS).*

# 5 Result of mesoscale simulations and the post-processing method

The post-processing of the mesoscale simulation is carried out in the following manner. First, a weighted mean of the wind class simulations results is calculated. This yields a simulated resource map. Second, for each wind class simulation, effects of elevation and roughness variation are removed with modules similar to those in the WAsP software. Then the weighted mean of the adjusted result from the wind simulations is made. This yields a wind atlas map, or generalized wind map for flat surface condition of a specified roughness. Figure 3 shows a schematic diagram of the wind class simulations and the post-processing steps.

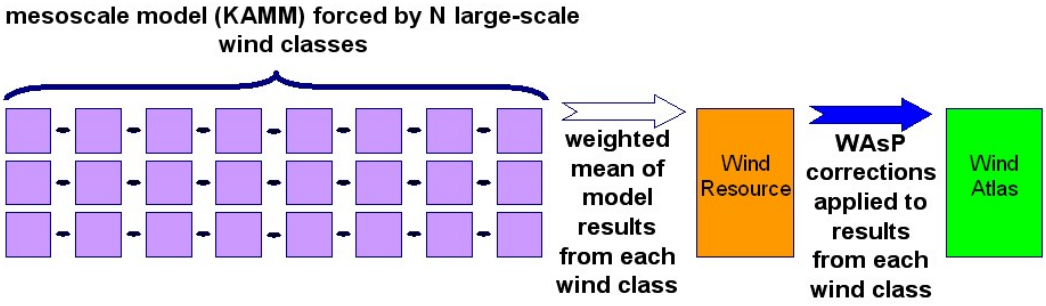


*Figure 3: A schematic diagram showing the KAMM/WAsP numerical wind atlas methodology.*

The mean **simulated** wind maps or wind resource maps give an overview impression of the variation of wind resources. The simulated wind maps for the three modelling domains giving mean annual wind speed and power density at 70 m are shown in Figure 4, and Figure 5, respectively. For the parts of the map which are covered by overlapping modelling domains, a weighted average of the contributing domains is made. The grid point weighting of each domain's result is a function of the proximity of the grid point to the domain boundary.

It must be remembered that for any location on the map one would not expect necessarily to have measured the same mean wind speed indicated by the map. This is because the map has been created using a surface description at 5 km resolution. In reality the surface will be full of details in surface elevation and surface roughness. For example, small hills and forests, pertaining to elevation and surface roughness details respectively, will not be resolved.

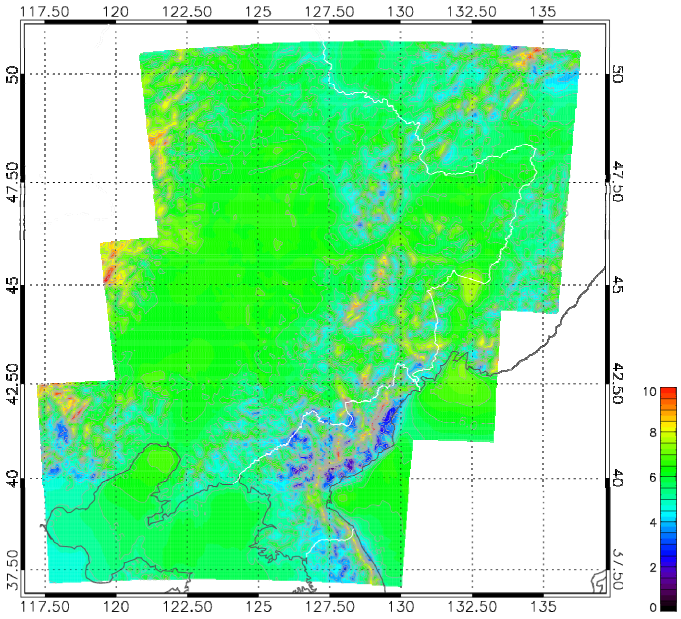


*Figure 4: Mean simulated wind speed at 70 m. The contour interval is 0.5 m/s.*

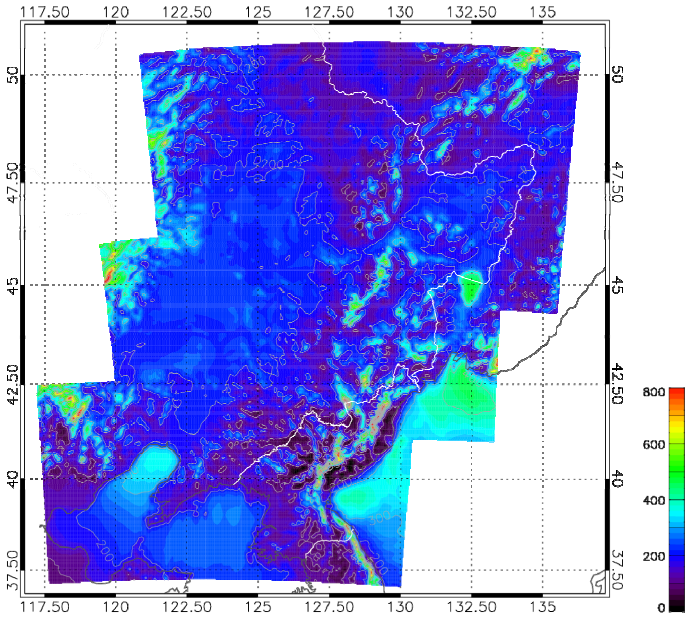


*Figure 5: Mean simulated wind power density at 70 m. The contour interval is 100 W/m$^2$.*

The problem, created by the limit in the surface description resolution, impacts all numerical wind atlas methodologies. However the KAMM/WAsP method, because of the *.lib-files* creation feature, allows detailed information about the surface elevation and roughness at a site of interest to be added using the WAsP software.

The mean **generalized** wind maps show the resource when the effects of resolved surface elevation and roughness change are removed. It shows what the annual mean wind speed would be for **flat** terrain with a **uniform** roughness of 3 cm. These kinds of map are useful because they show the mesoscale influence on wind resource, i.e. variation of resource due to phenomena other than local orographic speed-up and

roughness change. The generalized wind speed and wind power density maps are shown in Figure 6 and Figure 7 respectively.

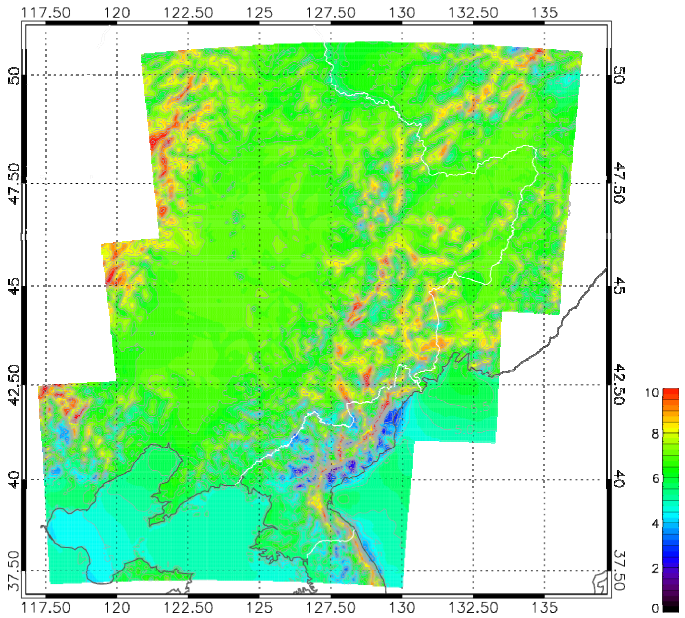


*Figure 6: Mean generalized wind speed at 50 m a.g.l. for 0.03 m roughness. The contour interval is 0.5 m/s.*

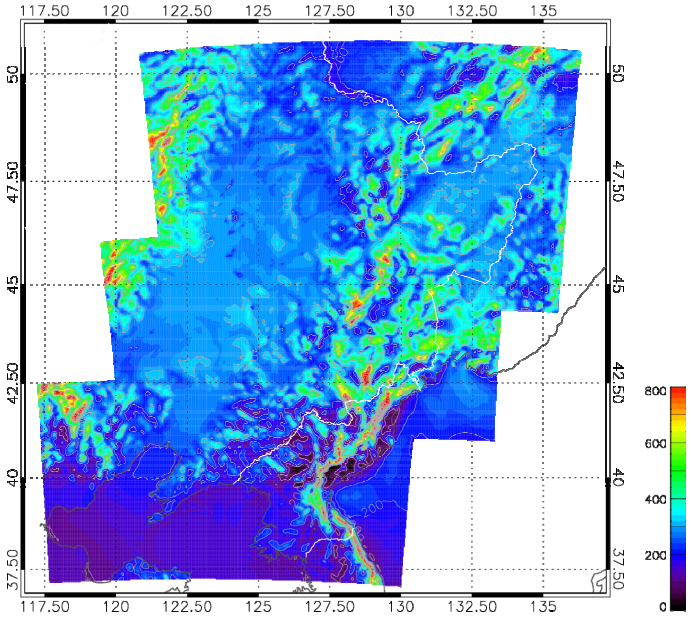


*Figure 7: Mean generalized wind power density at 70 m a.g.l. for 0.03 m roughness. The contour interval is 100 W/m2.*

Figures corresponding to Figure 4, Figure 5, Figure 6 and Figure 7 but with a larger format are given in Section 19 (Appendix A). Data files for the maps are also available, see Sectoin 20 (Appendix B)

# 6 Error and uncertainty

The uncertainty or error on the final results of the numerical wind atlas methodology should be considered as part of the study. Each step in the methodology involves approximations and uncertainties, therefore the estimation of the final uncertainty must consider how each step may contribute to the uncertainty and characterize the impact of the error. Contributors to the errors may include:

**Description of the large scale meteorological conditions from the NCEP/NCAR reanalysis.**

- The global NCEP/NCAR reanalysis uses a rather coarse resolution and its accuracy is higher in regions of high density observations. In regions of scarcer measurement the accuracy is degraded.
- Errors in the wind velocities may lead directly to errors in wind resource
- Errors in temperature profiles will lead to errors in stability and Froude number, and may give rise to spurious flow behaviour in complex terrain.

**Determination of the wind class and their associated vertical profiles of geostrophic wind and temperature.**

- Breaking down a large amount of atmospheric data into between 100 and 150 different wind classes is a way to reduce the amount of computer resource necessary to perform the mesoscale simulations. In doing so, it is possible that new sources of error are added in the process. However, great care has been taken to develop the method in which the wind classes are determined to minimize this error.
- Certain choices for the properties of the wind classes must be made. For example, at what height should the geostrophic wind be used to define the wind classes. Careful and appropriate selection of such properties minimizes error from this step.

**Description of the surface elevation**

- The surface elevation errors may come about due to insufficient spatial resolution. One of the most serious consequences of an error in the orography is the under-representation of high terrain. For example the heights of peaks are reduced when a lower resolution is used. This may lead to incorrect interaction of flow with terrain.

**Description of the surface roughness**

- The surface roughness errors may come about due to insufficient spatial resolution, and also through incorrect estimation of roughness length.

**Mesoscale modelling**

- Thermally driven winds, such as sea breezes, are known to be difficult to reproduce in the mesoscale model. Since the temperatures for land and sea surfaces are held fixed in time for each wind class it is expected that evolution of such wind phenomena are not reproduced.

- The KAMM modelling assumes a uniform and steady atmospheric forcing, thus any wind features due to transient and spatially varying forcings are not accounted for well.

**Microscale modelling**

- By accounting for the local mesoscale orographic speed-up and roughness change it is possible to transform the simulation wind characteristics to generalized wind characteristics (WAsP *.lib-files*). This process may introduce some uncertainties to the generalized wind statistics. This may be more problematic in areas of complex terrain and roughness change.
- The vertical profile of wind velocity is determined with an assumed surface heat flux climatology. The extent to which the assumed surface heat flux climatology is appropriate for specific locations will have an influence on the uncertainty of the results.

Typically numerical wind atlas studies using the KAMM/WAsP method and employing verification have demonstrated uncertainty on annual mean wind speeds of between 5% and 15% (Mortensen et al, 2005 and Frank et al, 2001).

# 7 Sensitivity to meteorological input

## 7.1 Temporal resolution for wind classification

We take advantages of the high temporal resolution measurements to investigate how temporal resolution would affect the wind classification.

The wind classification is not exactly the same as used in the KAMM/WAsP method. Here, the parameters that are used for wind classification are: wind speed, wind direction and the Bulk Richardson number, RiB, between 10 and 69 m. Data are classified in 12 wind sectors (345 – 15, 15 – 45 etc.), 4 wind speed ranges (0 – 0.5<u>, 0.5<u> – 1.2<u>, 1.2<u> – 2<u> > 2<u> , where <u> is the mean wind speed), 3 stability conditions (unstable RiB<-0.15, neutral -0.15< RiB<0.1, stable RiB>0.1).

Data from masts with large coverage of wind and temperature are used. Weighted mean with different sampling rates are compared with 10 min values. The sampling rates examined are 10 min, 1 h, 3 h, 6 h, 12 h and 24 h, where 6 h is mostly interesting for the KAMM/WAsP method and 24 h could be interesting for the CMA method.

The dependence of the weighted mean wind on the sampling rate is shown in Figure 8 at m02, m08 and m09. Station m02 is in coastal zone, station m08 is in complex terrain and station m09 is in a relatively flat area. The data suggest a sampling rate not longer than 6 hours should be used. When the sampling rate is larger than 12 hours, the uncertainty, calculated as $(u_{max}-u_{min})/u_{mean}$, is largest at the complex terrain m08. The diurnal variation is smaller at the coastal site m02, although still existing (see the spectra below), this gives rather flat variation for sampling rate between 12 – 24 hours.

In the KAMM/WAsP method, the wind class is defined according to the 6-h NCEP/NCAR reanalysis data. This study suggests using 6-h data is not a problem in defining wind classes.

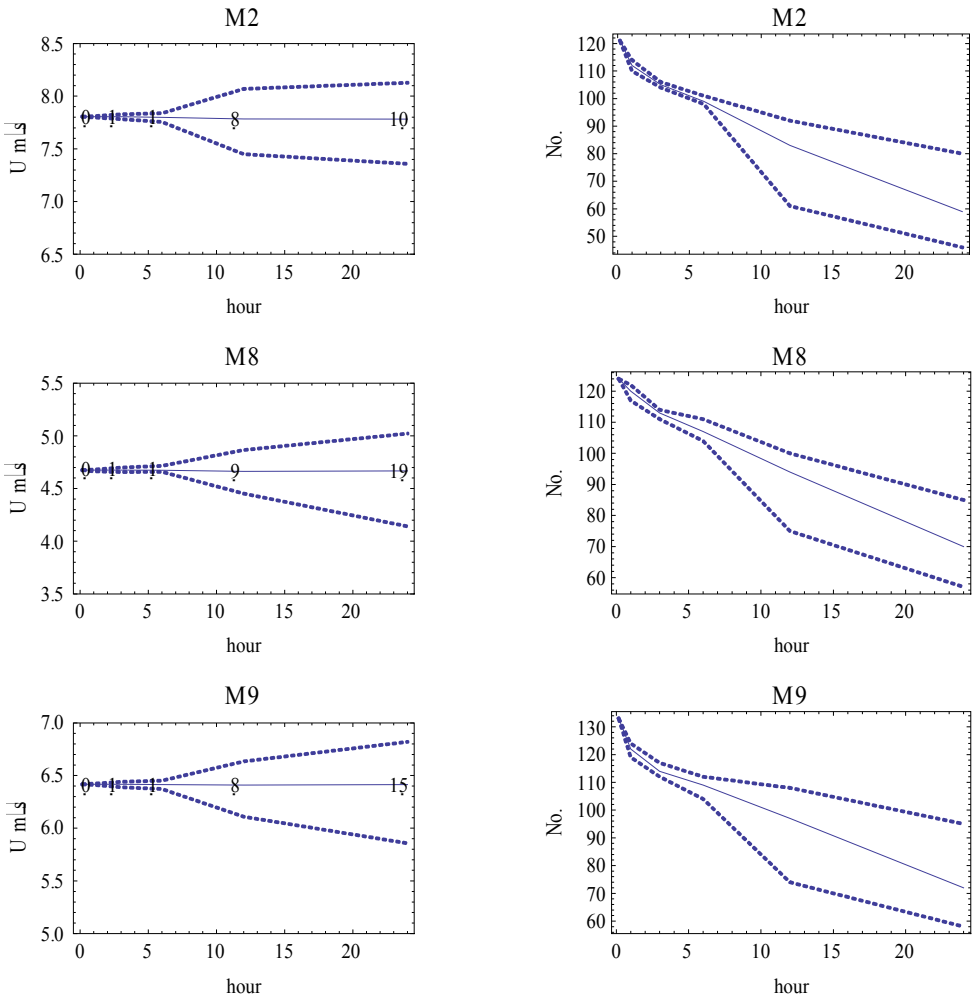


*Figure 8: Weighted mean wind speed (left column) and numbers of classes (right column) according to wind classification as a function of sampling rate from 10 min to 24 hours. Solid lines are the mean value and the dashed curves give the min and max mean wind speed. The numbers are* $(u\_{max}\text{-}u\_{min})/u_{mean}$ *printed at corresponding sampling rates.*

Spectral analysis is performed at the same time at all sites. Figure 9 shows dominant peaks at 1 and 2 day$^{-1}$ at station m08 and m09, suggesting sampling rates lower than twice a day will miss the diurnal variation. The peaks at higher levels are normally less dominant due to less surface impact and sometimes they disappear, e.g. at station m02 near the coast.

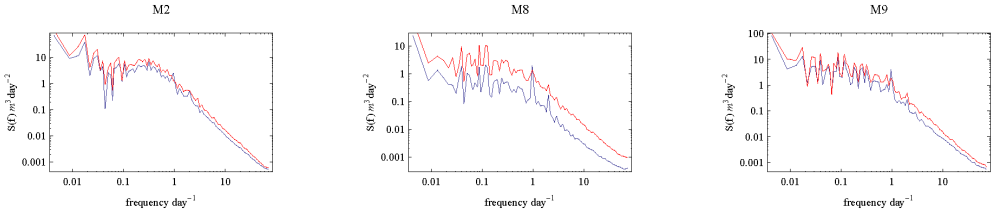


*Figure 9: Spectrum of wind speed at 10 m (blue) and 70 m (red), at stations m02, m08 and m09.*

## 7.2 The spatial variations of the geostrophic wind and the generalized wind, and their indication for defining KAMM-domain size

The wind classification is also done with generalized winds from stations where wind and temperature are both available. Speed-up coefficients from terrain and roughness are obtained from WAsP. The wind classification is not very different from that made with actual wind.

The correlation coefficients of the generalized winds is calculated with the geostrophic drag law between different sites are calculated within the three domains (between m01, m02 and m03; m04, m05 and m06; m07, m08 and m09). Good correlation of the standard wind exits between m04, m05 and m06 (correlation coefficients (cc) are: cc(m04,m06) = 0.54, cc(m04,m05)=0.70, cc(m06,m05)=0.68), probably because of the relatively similar terrains and closer distance compared to the other station groupings. The correlation is worse for m01 and m02 (0.31) and almost none for m01 and m03. The standard winds at m07, m08 and m09 are almost not correlated – the distance between them is also larger than that between stations in other domains.

Next, correlation coefficients of the geostrophic wind, G, (from NCEP/NCAR reanalysis) between the grid points close to the 9 stations and the rest of the grid points in the domain are calculated, and shown in Figure 10. The general pattern is quite consistent: there is a decrease of the correlation in G from 1 to 0.8 at a distance of 250 km (approximately the reanalysis grid resolution) and to 0.6 at about 500 km. This might be used as an indication that when using wind class from one grid point for the entire model domain, the domain should not be too big to avoid situations where large scale winds are not correlated.

Correlation coefficients between time series of G and the generalized winds at several stations are calculated, e.g. cc(m02)=0.37, cc(m04)=0.42, cc(m08)=0.37 and cc(m09)=0.52. Seemingly there is a tendency that G and generalized wind are better correlated in simple terrains. The discrepancy between G (synoptical) and the generalized wind (WAsP domain scale) can be considered as a measure of the importance of the mesoscale effect.

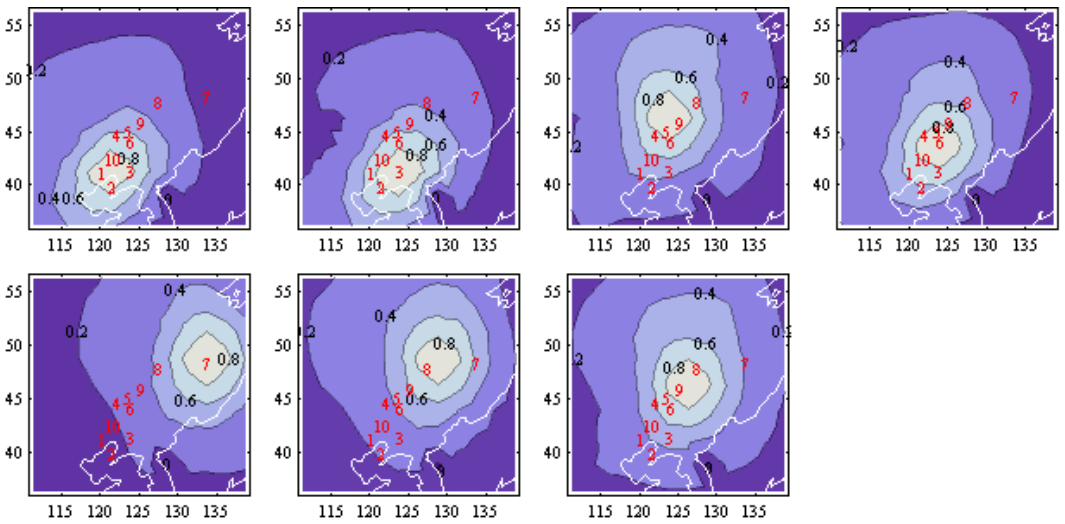

*Figure 10: Correlation coefficients of geostrophic wind, G, between NCEP/NCAR reanalysis grid points close to the stations and the rest of the grid points in the domain. Red numbers 1-10 mark the positions of the 10 stations.*

## 7.3 Calculation of geostrophic wind

We tried three different methods to calculate the mean geostrophic wind since 1979, <G>. In the KAMM/WAsP method, it is not <G> but a number of ranges of G with different direction and stability conditions that are used. <G> is examined here simply to test if it is sensitive to use different reanalysis datasets or different ways of obtaining G.

Table 2 lists some of the data details. The first method is using NCEP/NCAR reanalysis geopotential height at 1000 mb. The second method is using NCEP/NCAR reanalysis surface pressure and temperature at 2 m to obtain mean sea level pressure ($P_{msl}$) and then G. The third method is using ECMWF reanalysis (ERA-40) mean sea level pressure to obtain <G>.

*Table 2: data that are used for calculating mean G.*

| Method | Data | Resolution | Data period |
|---|---|---|---|
| 1 | NCEP/NCAR reanalysis geopotential height at 1000 mb | 2.5° | 1979 – 2009 |
| 2 | NCEP/NCAR $P_s$ and $T_{2m}$ to obtain $P_{msl}$ | 1.91° | 1979 – 2009 |
| 3 | ECMWF reanalysis (ERA-40) $P_{msl}$ | 2.5° | 1979 – 2001 |

All methods work best in low elevations and poorest over high terrains with significant elevation gradient. Compared to $P_{msl}$, geopotential heights at 1000 mb is about 100 m higher up and using it for G is less affected by terrain variations. However, over terrains comparable to or higher than 1000 mb, it could still be an issue (i.e. at m03 and m08, the mesoscale elevations are 672 m and 341 m). In general circulation models, when reducing pressure to the mean sea level, hydrostatic balance is often used and it is suggested that this reduction is mostly valid for areas with elevation lower than about 300 m.

The distribution of <G> with longitude and latitude from the three methods is presented in Figure 11, Figure 12 and Figure 13. The background magnitude of <G> over the three Northeast provinces is comparable, with method 2 giving 1 m/s larger. This could be a result of its finer resolution. Due to the above mentioned issues in the calculation of G, method 2 is expected to be more sensitive to the high elevations, and it is reflected clearly in Figure 12. In these areas, using method 2 gives larger uncertainty.

In short, over the three provinces, the three methods suggest rather consistent mean <G>.

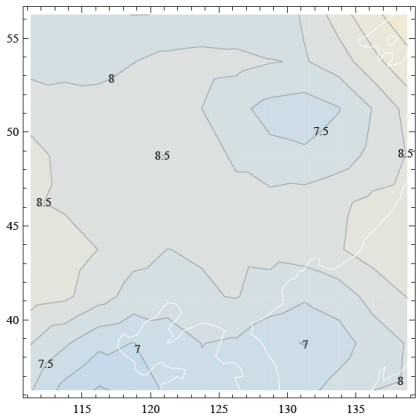


*Figure 11: <G> calculated with method 1, see Table 2.*

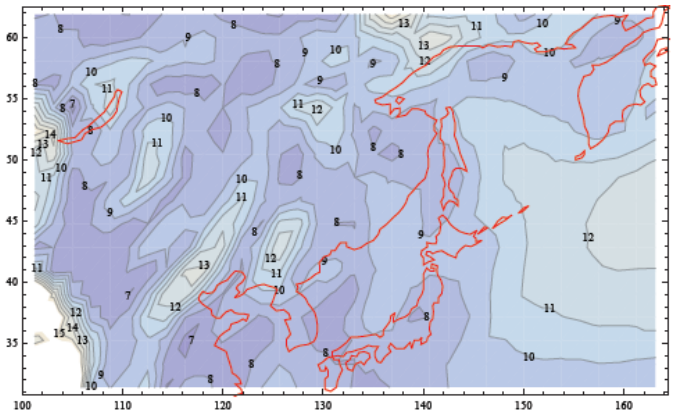


*Figure 12: <G> calculated with method 2, see Table 2.*

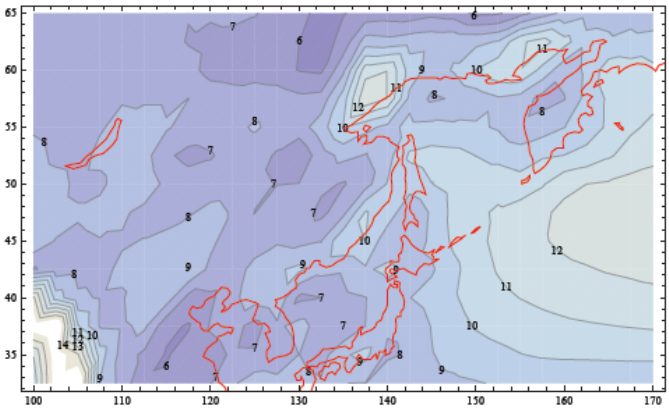


*Figure 13: <G> calculated with method 3, see Table 2.*

# 8 Sensitivity testing in Harbin test area

During the 3-week mesoscale training workshop at Risø DTU in 2008, KAMM/WAsP mesoscale modelling was carried out for a 600 x 600 km test area, centred around Harbin. The area is interesting as it features diverse orography featuring some high elevation, a gap, and level plain areas, see Figure 14.

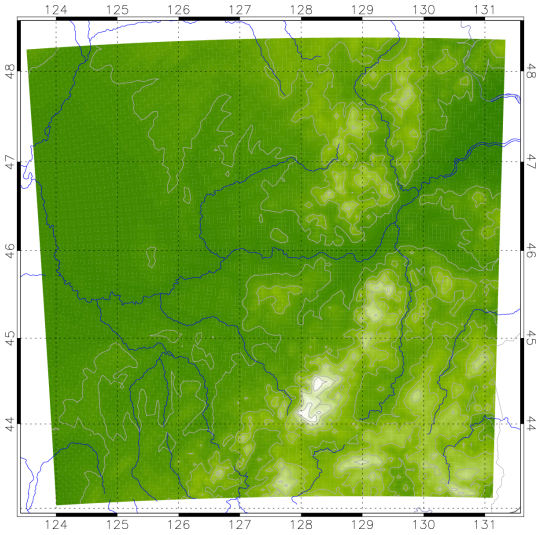


*Figure 14:Map showing the orography for the Harbin test area. The contour interval is 100 m.*

The wind resource was first calculated using a wind class set defined by geostrophic winds at 0m at 128.75E 46.25N, using 12 direction sectors and 2 stability classes. The number of wind classes in this wind class set was 121. These wind classes are referred to as the control wind class set. Calculating the wind resources using these wind classes at a model resolution of 5 km gives the wind resource map show in Figure 15.

It was of interest to see to what extent the wind resource altered when different sets of wind classes were employed. First wind class sets were determined using different number of stability classes. Using one stability class gave a set with 68 wind classes. Using 3 stability classes gave a set with 156 wind classes. These additional wind class set were used to calculate wind resource maps. The data for the two sets of wind classes plus the control set, 345 wind classes in all, were used to create an ensemble mean of the wind resource. Moreover the spread of the ensemble, given by the standard deviation of the wind resource map for any given grid point on the map, was calculated. The ensemble mean and spread are show in Figure 16.

Next wind class sets were determined using different number of direction sectors. Using 8 direction sectors gave a set with 88 wind classes. Using 18 direction sectors gave 157 wind classes. Again these wind class sets were used to calculate the wind resource for the test area. These two wind class sets plus the control totals 366 wind classes. Figure 17 shows the ensemble mean and spread given using these three sets.

The conclusion from these studies was that sensitivity to the use of wind class sets was rather subtle. The changes overall were small, but some areas of the calculation domain

were more sensitive to the changes in wind class sets. These areas tended to be in the slope areas of elevated and more complicated terrain.

Figure 16 shows that sensitivity to stability class number is mainly apparent in low wind areas. Figure 17 shows that sensitivity to number of direction sectors is smaller than sensitivity to stability class number, and again concentrated in the low wind areas of the modelling domain.

The method of testing the sensitivity was considered valuable and worthy of expansion for the whole region to be mapped. Results from these sensitivity experiments will be given in Section 9.

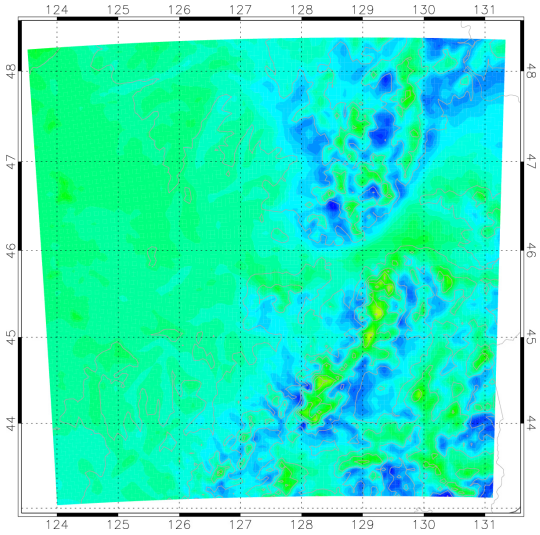


*Figure 15: Mean simulated wind at 50 m for the Harbin test area using 121 wind classes.*

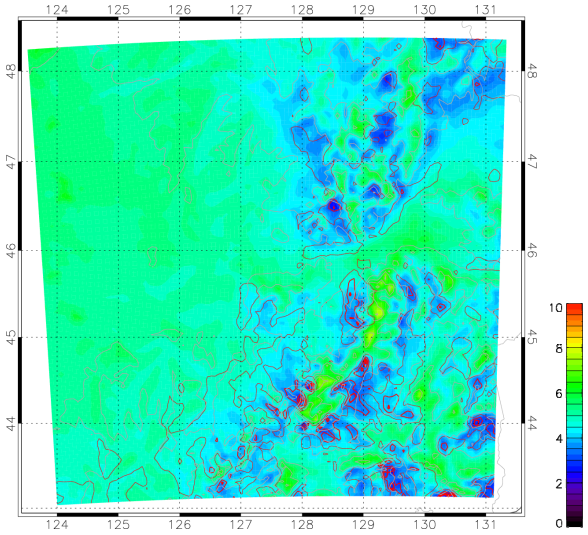


*Figure 16: Ensemble mean simulated wind at 50 m for the Harbin test area using 3 sets of wind classes (345 wind classes) using different number of stability classes (1,2,and 3). The red contours indicated the spread of the ensemble (standard deviation). In order of increasing thickness the contours represent spread of 1.5, 3, and 6 % of the ensemble mean.*

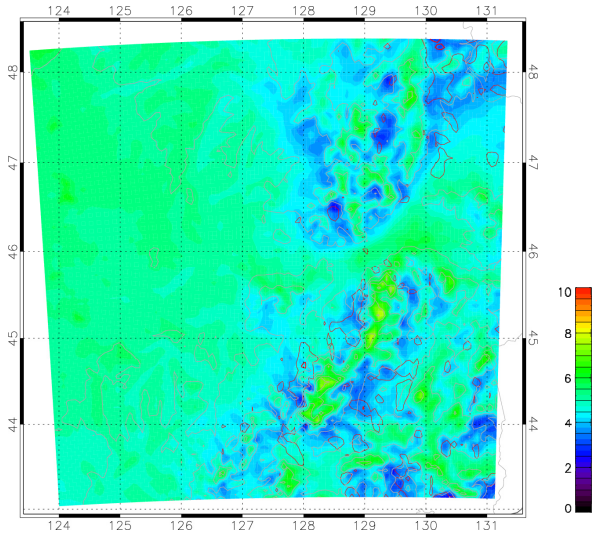


*Figure 17: Ensemble mean simulated wind at 50 m for the Harbin test area using 3 sets of wind classes (366 wind classes) using different number of direction sectors (8,12,and 18). The red contours indicated the spread of the ensemble (standard deviation). In order of increasing thickness the contours represent spread of 1.5, 3, and 6 % of the ensemble mean.*

# 9 Sensitivity testing for modelling domains

Following the promising method for examining sensitivity for the test area around Harbin (Section 8), a much more comprehensive series of sensitivity studies was performed for the three modelling domains covering the area of interest.

The aspects to be tested were i. sensitivity to model resolution, ii. sensitivity to the changes in the wind classification system, iii. sensitivity to surface roughness, iv. sensitivity to surface temperature configuration. These aspects are addressed in the following subsections. In each subsection only the figures for the centre domain are given in the main text, while the figures for the northern and southern domain are given in the appendix. This is done simply to reduce the number of figures appearing in the main text.

## 9.1 Sensitivity to model resolution

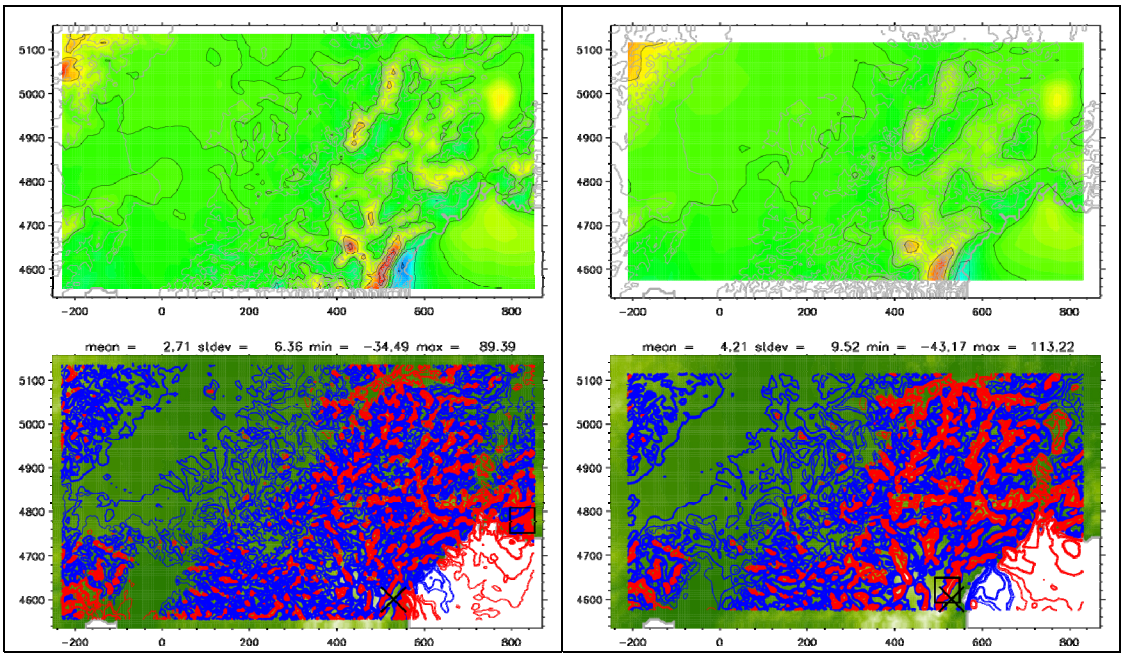


*Figure 18: Maps of mean simulated wind speed at 100 m (upper panels) for 10 km (left) and 20 km (right) resolution mesoscale modelling for the centre domain. The lower panels show the difference compared to the 'control' resolution of 5 km. Red contours indicate negative differences, blue contours positive differences. Contours increase in absolute value with increasing thickness, going from 1, 2, 4, 8, 16 %. Statistics for the differences in % are given above the difference maps.*

Using the wind class sets, shown in Figure 2, the numerical wind atlas calculation was carried out using mesoscale modelling at 20 km and 10 km for the three modelling domains. The results of the coarse resolution mesoscale modelling were then compared to the results from the 5 km mesoscale modelling.

For the centre domain, northern domain, Figure 18, and Figure 47, lower resolution increases the resource regionally by about 2.5 % and 3.5 % for resolutions 10 and 20 km

respectively. However, differences locally can be very large. For example, on elevated peaks the wind resource is reduced, and in the gap region near Harbin the wind speeds are lowered, as the gap itself becomes poorly represented at lower resolutions and may in effect becomes more closed.

For the southern domain, Figure 49, lower resolution increases resource regionally, 1.7 % and 3.7 % for resolutions 10 and 20 km respectively. Lower values here may be due to larger portion of sea area in the domain. The strait shows a reduced resource with lower resolution, as in effect the strait is narrowed by the coarse resolution. Other coastal effects are seen which may be related to coarse resolution reducing barrier jet type wind enhancements, due to barrier topography being poorly resolved and of lower elevation.

## 9.2 Sensitivity to the wind classification system

There are three parts to the investigation into sensitivities to differences in the wind classification system. First, the locations and height, where the wind classes are defined are altered. Second, the number of stability classes is altered. Thirdly, the importance of the number of wind classes is tested.

First, the numerical wind atlas calculation was performed using 2 alternative sets of wind classes for each modelling domain. The first alternative wind class set uses geostrophic wind and temperature profiles determined at a different location, but still within the modelling domain, where the wind class definitions are determined. The second alternative wind class set uses the same location as the control wind class sets, but uses geostrophic winds at 1500 m instead of 0 m.

For the centre domain, northern domain and southern domain, Figure 20, Figure 47, and Figure 49, respectively, the regional effect of changing the horizontal or vertical location for the wind class definitions is rather small (<2%). However locally the differences can be quite large, i.e. tens of per cent (<40%). The largest effects being in the more complex terrain area. In the plain areas there is a tendency for reduced resource using the new horizontal location for wind class definitions, whereas in the same area there is an increased wind resource using the geostrophic wind at 1500 m for the wind class definitions. Interestingly, for the centre domain using the geostrophic wind at 1500 m for the wind class definitions gives a more complex pattern of changes to the resource in the offshore area.

Secondly, the wind classes are changed again by using 1 stability class and 3 stability classes. For the northern domain this gives 90 and 258 wind classes, for the centre domain, 82 and 251, and the southern domain 84 and 258, correspondingly.

For the central domain, northern domain, and southern domain, Figure 22, Figure 55, and Figure 57 respectively, the regional effect of changing the number of stability classes is very small (<1%). However locally the differences can be quite large, i.e. tens of per cent (<25%). The largest effects are found within areas of complex terrain, however not at highest parts of the terrain, but rather in the adjacent slopes. Interestingly, there can be complex patterns of changes of resource in the offshore areas to the east of the continent, but almost not changes in the offshore resources south of Dongbei.

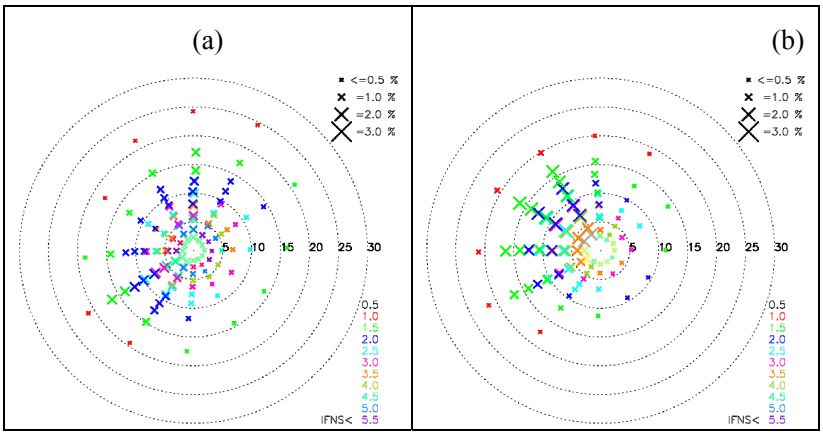


*Figure 19: (a) Wind class set 'NC_11' based on geostrophic winds at 0m at 128.75E 43.25N and (b) wind class set 'NC_20' based on geostrophic winds at 1500 m at 123.75E 43.75N, used for the centre domain.*

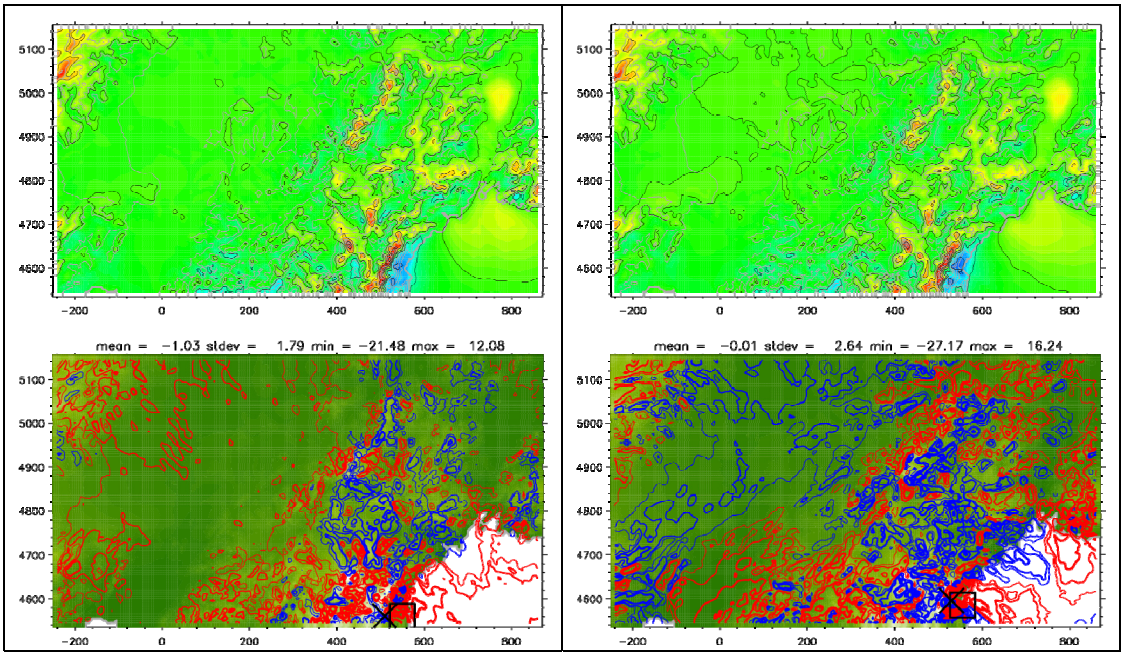


*Figure 20: Maps of mean simulated wind speed at 100 m (upper panels) using wind class set 'NC_11' defined at a different horizontal location (left) and wind class set 'NC_20' defined at a different vertical location (right) for the centre domain. The lower panels show the difference compared to the 'control' wind class set. Red contours indicate negative differences, blue contours positive differences. Contours increase in absolute value with increasing thickness, going from 1, 2, 4, 8, 16 %. Statistics for the differences in % are given above the difference maps.*

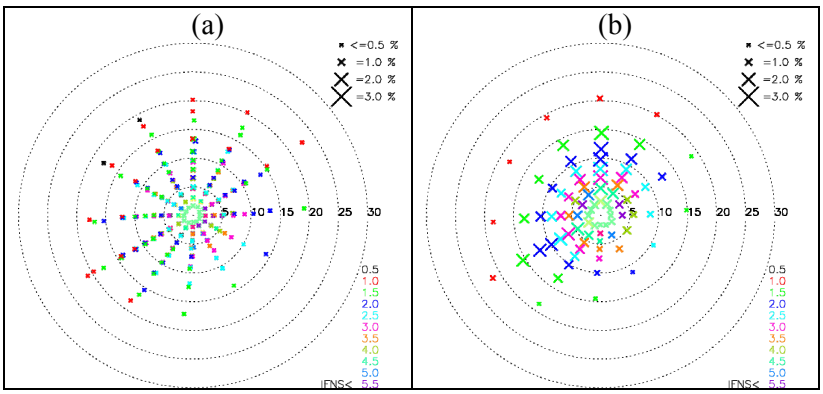


*Figure 21: (a) Wind class set 'NC_30' using 3 stability classes and (b) wind class set 'NC_40' based on 1 stability class, used for the centre domain.*

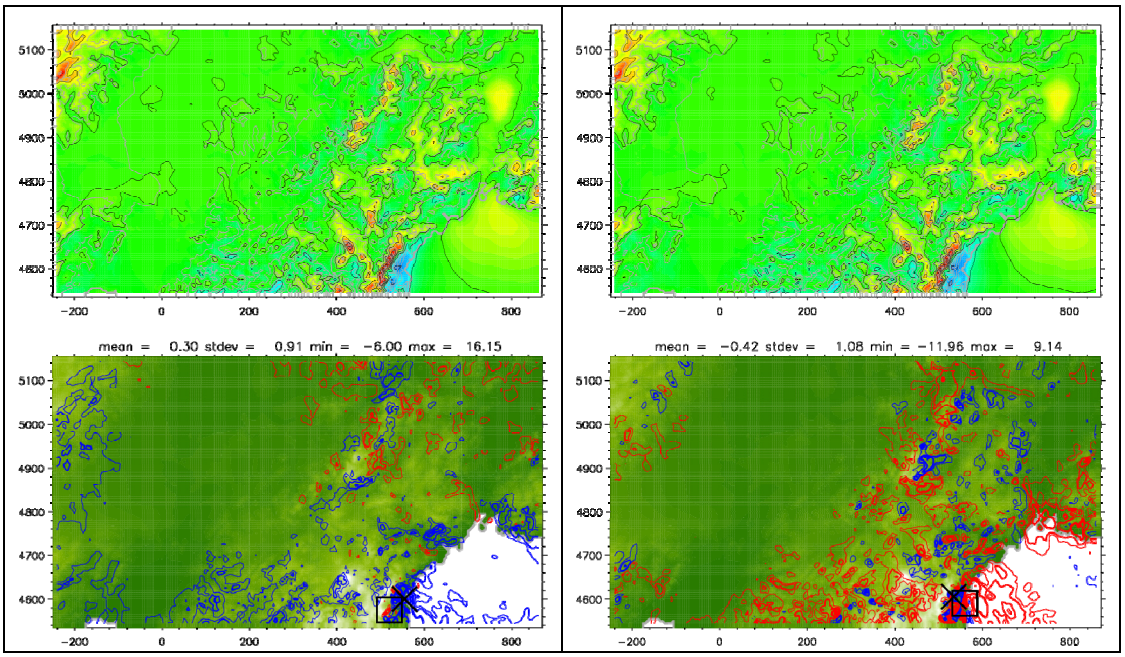


*Figure 22: Maps of mean simulated wind speed at 100 m (upper panels) using wind class set 'NC_30' based on 3 stability classes wind (left) and wind class set 'NC_40' based on 1 stability class (right) for the centre domain. The lower panels show the difference compared to the 'control' wind class set. Red contours indicate negative differences, blue contours positive differences. Contours increase in absolute value with increasing thickness, going from 1, 2, 4, 8, 16 %. Statistics for the differences in % are given above the difference maps.*

Thirdly, we are interested in investigating the impacts of representing the large scale climate in three ways, two ways use approximately the same large number of wind classes climate, one including stability for class definitions (3 stability classes) the other ignoring stability for class definitions (1 stability class). The third way representing the large scale climate is with a low number of wind classes and ignoring the stability effects.

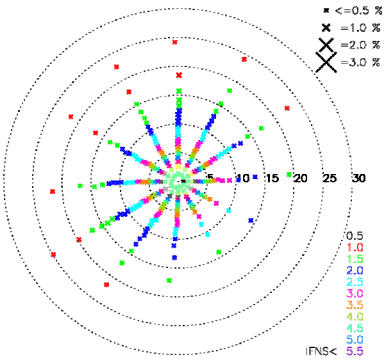


*Figure 23: Wind class set 'NC_50' using 1 stability class, used for the centre domain.*

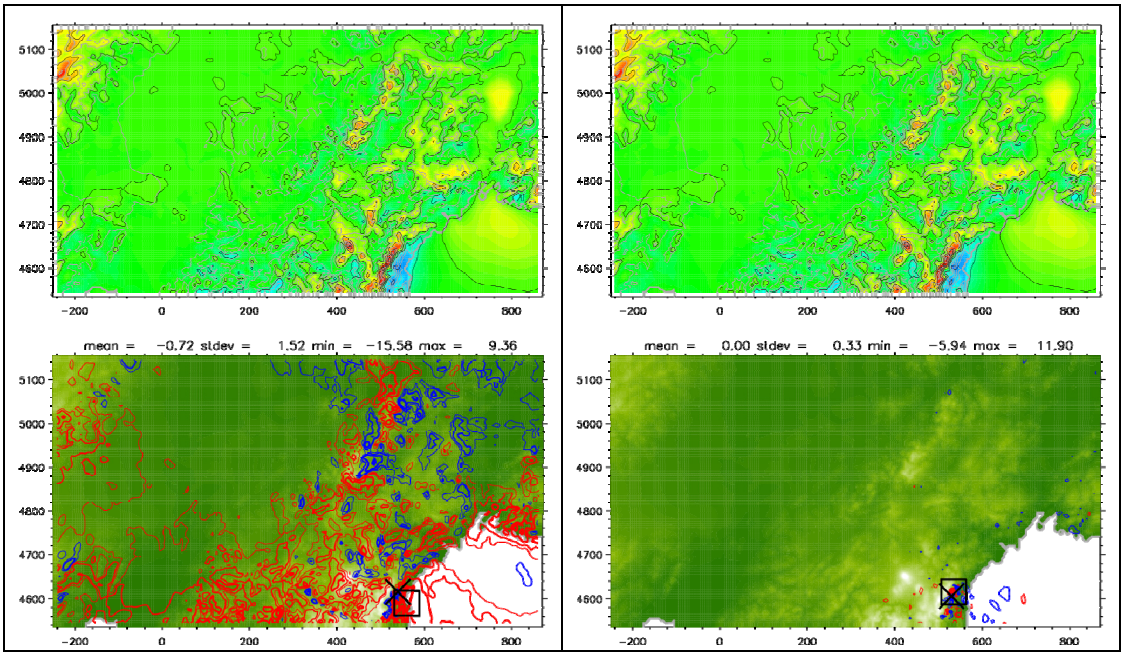


*Figure 24: Maps of mean simulated wind speed at 100 m (upper panels) using wind class set 'NC_50' based on 1 stability class wind (left and right) for the centre domain. The lower panels show the difference compared to a wind class set 'NC_30' based on 3 stability classes (left) and compared to a wind class set 'NC_40' based on 1 stability class but reduced number of wind classes. Red contours indicate negative differences, blue contours positive differences. Contours increase in absolute value with increasing thickness, going from 1, 2, 4, 8, 16 %. Statistics for the differences in % are given above the difference maps.*

For the centre domain, northern domain and southern domain, Figure 24, Figure 55, and Figure 57, respectively, it can be seen that including stability compared to excluding stability, even with a large number of wind classes, has a similar effect to what was seen when 1 stability class with few wind classes was used. This is confirmed by looking at the right column maps. These maps show the impact of representing the large scale climate with few wind classes compared to many wind classes, but in both cases ignoring stability in the wind class definitions. The regional impact is very small (<0.2%), and it is only in very localized areas occupying only a small part of the domain that the impact approaches anything large (<12%). This is interesting as it demonstrates that over most of the domains increasing the number of wind classes by approximately a factor 4 makes very little difference, if stability is ignored in the wind class definitions.

## 9.3 Sensitivity to surface roughness length

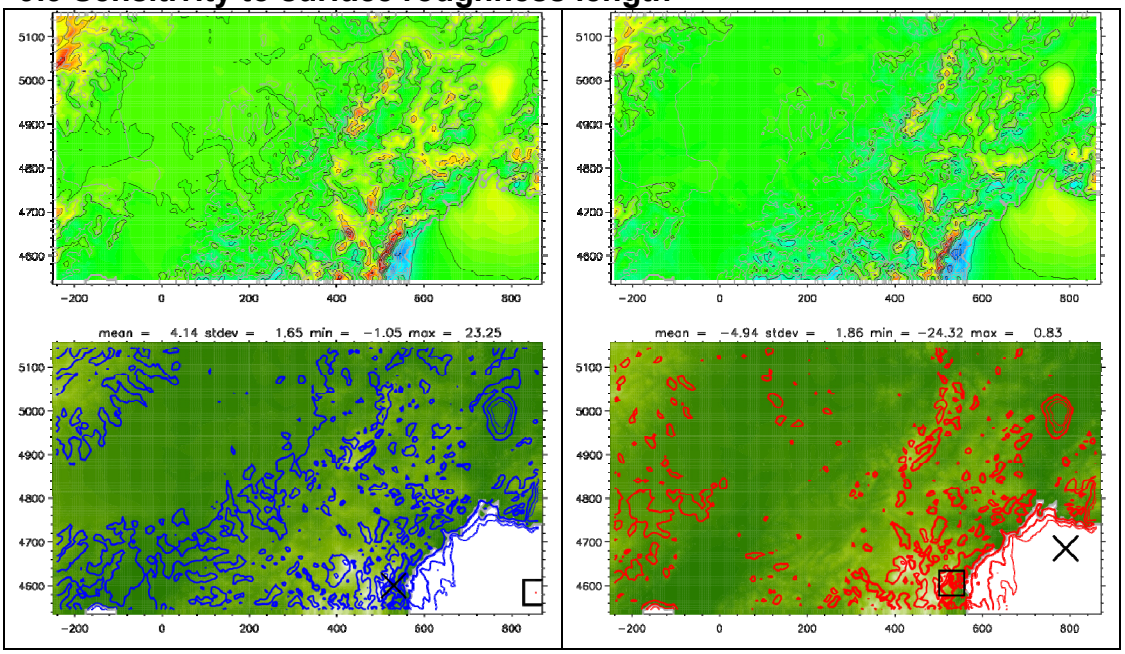


*Figure 25: Maps of mean simulated wind speed at 100 m (upper panels) where land roughness lengths are halved (left) and where land roughness lengths are doubled (right) for the centre domain. The lower panels show the difference compared to the 'control' using nominal roughness lengths.*

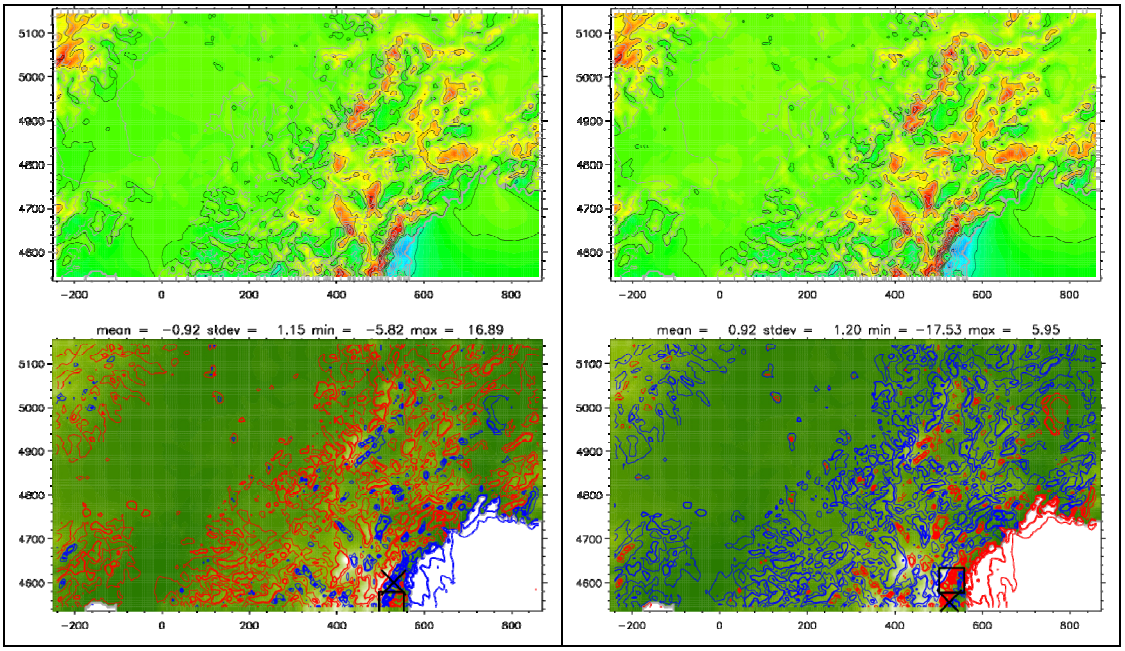


*Figure 26: Maps of generalized wind speed at 100 m (upper panels) where land roughness lengths are halved (left) and where land roughness lengths are doubled (right) for the centre domain. The lower panels show the difference compared to the 'control' using nominal roughness lengths. Red contours indicate negative differences, blue contours positive differences. Contours increase in absolute value with increasing thickness, going from 1, 2, 4, 8, 16 %. Statistics for the differences in % are given above the difference maps.*

In this test two further numerical wind atlases are calculated for each domain in which the surface roughness used for land surface either halved or doubled. This tests the sensitivity of the wind resource calculation to a sizable change in the roughness length.

For the centre domain, northern domain and southern domain, Figure 25, Figure 58, and Figure 60, respectively, halving land surface roughness increased wind resource regionally, and doubling land surface roughness decreases wind resource regionally. This effect is about 5% in each case. For the southern domain the effect is slightly reduced because of the large unchanged sea roughness. Interestingly, locally there can be decreases in resource for the lower land roughness cases (<2%), and higher resources for the higher land roughness cases (<4%).

Now when the post-processing is carried out to a large extent the regional change in the wind resource due to alteration in the land surface roughness is removed. For the centre domain, northern domain, and southern domain, Figure 26, Figure 59, and Figure 61, respectively, the regional effect of halving or doubling land surface length is regionally less than 1.2%. Along coastal areas the effect can be somewhat stronger and in some limited locations the effect can be as large as 18%.

## 9.4 Sensitivity to surface temperature

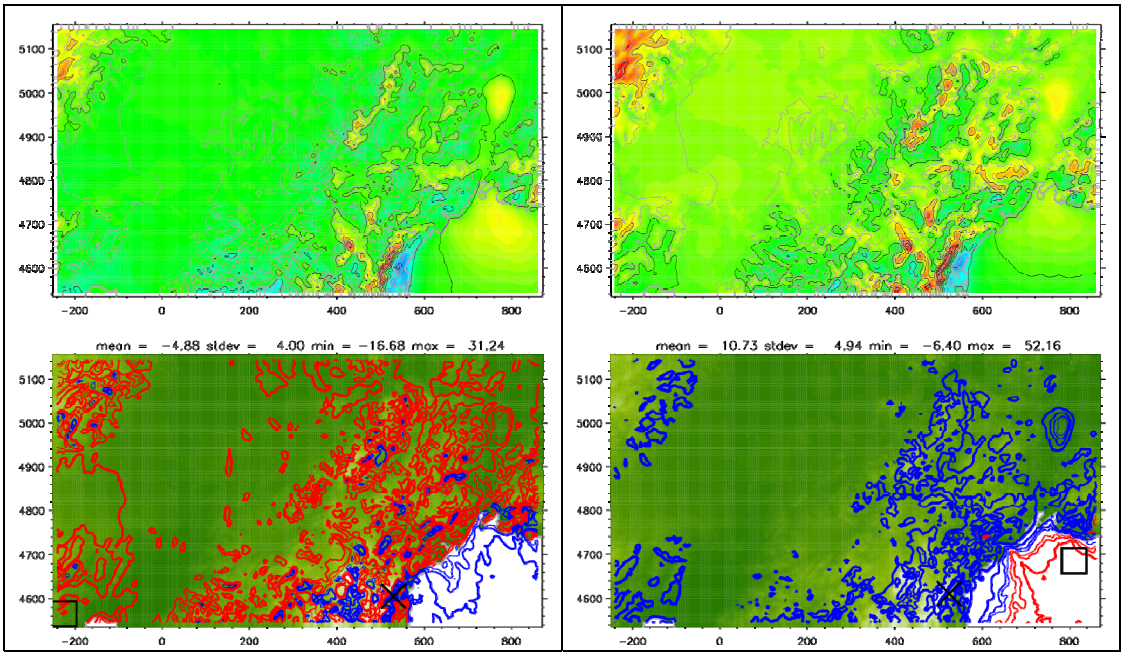


*Figure 27: Maps of mean simulated wind speed at 100 m (upper panels) for warm-land / cool-sea configuration (left) and for cool-land / warm-sea configuration (right) for the centre domain. The lower panels show the difference compared to the 'control' configuration with surface surface-air temperature equilibrium at initial time. Red contours indicate negative differences, blue contours positive differences. Contours increase in absolute value with increasing thickness, going from 1, 2, 4, 8, 16 %. Statistics for the differences in % are given above the difference maps.*

In this test two further numerical wind atlases are calculated for each domain in which the surface temperature configuration is changed to either warm-land / cool-sea or cool-land / warm-sea. The surface temperature is offset from the lowest model air temperature at each grid point by a constant values for sea and land. The offset is ±4.5 K. This tests the sensitivity of the wind resource calculation to changes surface temperature and the associated changes in the surface heat fluxes, thus changing the modelled stability characteristics.

For the centre domain, northern domain and southern domain, Figure 27, Figure 62 and Figure 63, respectively, the warm-land/cool-sea configuration decreases the on-land wind resource regionally, and the cold-land/warm-sea configuration increases the on-land wind resource regionally. The all land northern domain best demonstrates this with a 9% decrease and a 12% increase for the warmer-land and cooler-land configurations, respectively. For the centre domain, and southern domain the warm-land/cold-sea configuration has an abrupt and single sign effect (more resource) on the offshore wind resource. Whereas for the cold-land/warm-sea configuration the offshore effect is somewhat more gradual, long reaching, and of both signs (in general, more resource close to shore, less resource away from shore). It appears that at 100 m, a transition from an unstable to stable boundary layer occurs much more swiftly than a transition from a stable to unstable boundary layer.

Locally the effect of the warmer-land is to reduce the spatial variation in wind resource, such that their maxima are diminished and their minima are boosted. This can be understood in terms of reduced stability and increased Froude number leading to flow being less influenced by the grid scale orography and roughness length properties.

## 9.5 Summary

A summary of the main impacts of the sensitivity tests is given in Table 3. Although it is difficult to quantity the sensitivities against each other, a qualitative impression of the sensitivity impacts can be obtained. For example, using more wind speed classes, but ignoring stability in wind class definitions, has a lesser effect than introducing stability classes in the wind class definitions. In most cases the tests exposed the possibility of large sensitivities at specific locations. The most sensitive regions can be stated generally as being in mountain/hill terrain and/or coastal regions.

From these sensitivity tests we can conjecture that the errors introduced in the each phase of the methodology within the wind class system selection, roughness assignment, model resolution limitations, and surface temperature configurations, will lead to a larger uncertainty and error in mountain/hill terrain and/or coastal regions. This is reinforced in the results of the verification (Section 11) and an indexing of the mesoscale terrain complexity in relation to numerical wind atlas error (Section 12).

*Table 3: Summary of the KAMM/WAsP sensitivity test.*

| **Sensitivity test** | **Regional effect** | **Maximum effect** | **Locations of maximum effect** |
|---|---|---|---|
| Resolution | < 5% | ~100 % | Mountain/hill terrain, ridges, gaps, coastal regions |
| Class definition location | < 2 % | < 33 % | Mountain/hill terrain, some coastal regions |
| Class definition height | < 2 % | < 38 % | Mountain/hill terrain, coastal regions |
| Number of stability classes | < 1 % | < 22 % | Slopes of mountain/hill terrain |
| Wind class number | < 1% | < 12 % | Most complex terrain areas, and their vicinity including offshore |
| Surface roughness | < 6 %<br>< 2 % | < 25 %<br>< 18 % | Coastal or lake coastal regions<br>Coastal or lake coastal regions |
| Surface temperature | <13 % | < 82 % | Mountain/hill terrain and coastal regions |

# 10 Methods used to generalize mesoscale winds

There are currently four methods for post-processing the winds from the mesoscale modelling in order to create generalized winds at any model grid point. The methods are outlined below.

For methods 1 and 2 the wind direction and friction velocity are topographically corrected by the linear model LINCOM. The corrected friction velocity is used to calculate the geostrophic wind, G, using a stability dependent drag law based on Monin-Obukhov length. For method 1 the Monin-Obukhov length is determined from the mesoscale model variables. For method 2, the Monin-Obukhov length is prescribed. Then, for an effective upstream roughness length, friction velocity is calculated by an iterative method using the geostrophic drag law for neutral stratification. Then, assuming a neutral surface layer the wind speed at a single reference height is calculated (i.e. a log profile is used) for the effective upstream roughness length for the given mesoscale grid point.

For method 3 the wind speed and direction at a single height are obtained by interpolation of the winds at model levels. This wind is topographically corrected by LINCOM to give the wind direction for a single reference height for the effective upstream roughness length or the given mesoscale grid point.

For method 4 the wind speed and direction at several heights is obtained by interpolation of the winds at model levels. For each of these heights the topographical corrections are used to give wind direction at the heights of interest. Where the interpolation level is above the lowest model level, linear interpolation is used. If the interpolation level is above the highest model level retained for post-processing purposes, then linear extrapolation is used. Where the interpolation level is below the lowest model level, then extrapolation using a similarity function is used.

At this stage, we have for each simulation the wind speed and direction for a single height for a single roughness length for methods 1, 2, and 3. In method 4, we have the wind speed and direction for several heights of interest for a single roughness length.

The next stage is to calculate the generalized wind speed and direction at a number of heights and a number of roughness lengths. This is done using the geostrophic drag law using neutral conditions, and the wind speed and direction for the single height (method 1, 2, and 3), or for the various heights (method 4), as the starting point.

When this is done for all wind class simulations, sectorwise Weibull fitting is done for the distribution of generalized winds. A problem arises when the number of simulations is smaller than a few hundred because the Weibull fitting is poor due to the small sample size per sector. The problem is addressed with a method that interpolates winds between similar wind class simulations. The number of interpolated wind class simulations us user defined. Typically, interpolation is used to yield a data population 5 times larger than the simulation data for the Weibull fitting. Once the sectorwise Weibull A and k are determined, the WAsP stability corrections accounting for climatological effect of mean and variance of surface heat fluxes (different for land and sea) are applied. For this correction the upstream distance to the shore is used. Finally, the sectorwise Weibull A and k parameters and sector frequencies are output in the form of a WAsP lib-file.

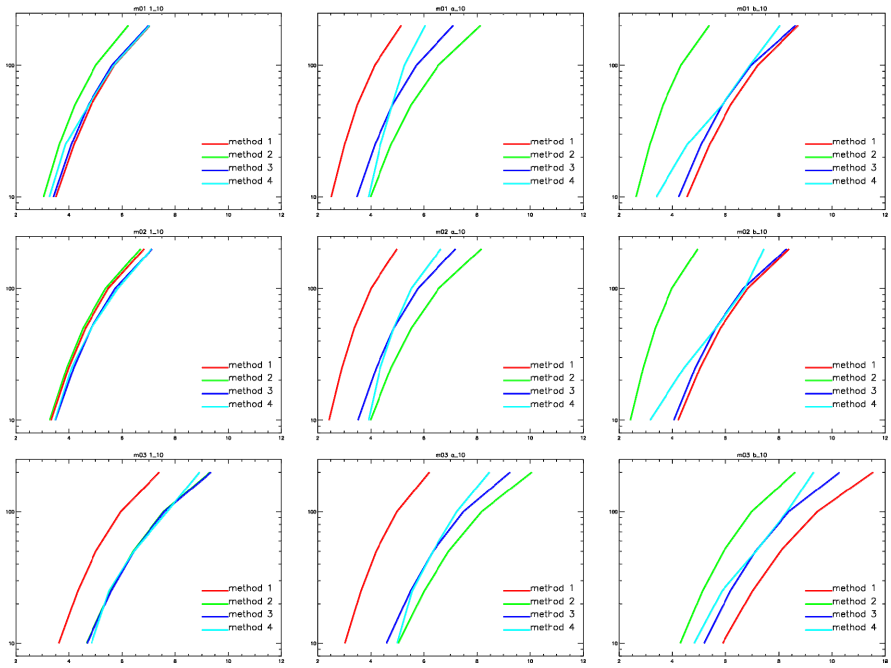


*Figure 28: The generalized wind profiles, height [m] vs wind speed [m/s], for station m01, m02, m03 (rows) using the control surface temperature configuration (left column), the warmer land / cooler sea configuration (centre column), and the cooler land / warmer sea configuration (right column). The coloured lines give the profiles given by different methods indicated by the legend.*

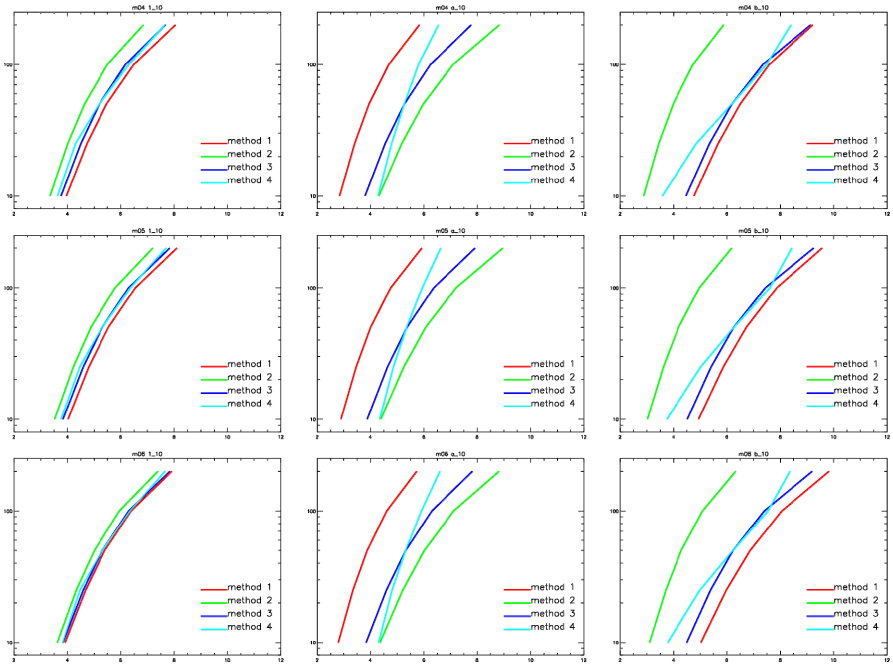


*Figure 29: The generalized wind profiles, height [m] vs wind speed [m/s], for station m04, m05, m06 (rows) using the control surface temperature configuration (left column), the warmer land / cooler sea configuration (centre column), and the cooler land / warmer sea configuration (right column). The coloured lines give the profiles given by different methods indicated by the legend.*

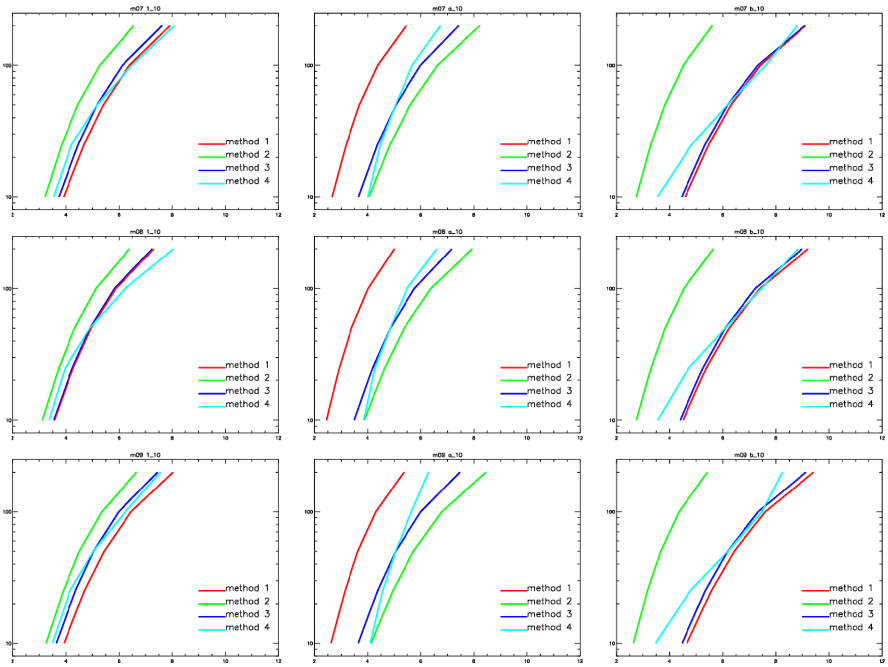


*Figure 30: The generalized wind profile, height [m] vs wind speed [m/s], for station m07, m08, m09 (rows) using the control surface temperature configuration (left column), the warmer land / cooler sea configuration (centre column), and the cooler land / warmer sea configuration (right column). The coloured lines give the profiles given by different methods indicated by the legend.*

Figure 28,

Figure 29 and Figure 30 show the generalized wind profiles calculated using the methods outlined above, for stations m01, m02, m03, and m04, m05, m06, and m07, m08, m09, respectively. These figures give the profile for three different surface temperature configurations of the mesoscale model (see Section 9.4). First we concentrate on the control configuration in which the surface and surface air temperatures are equal. In all these cases method 2 uses a prescribed value for the Monin-Obukhov length corresponding to neutral conditions. Note that the figures use a log height axis, therefore we would expect a neutral profile to give a straight line. In nearly all cases the profiles flatten slightly with height indicating slightly stable profiles. This is due to the WAsP stability correction.

Examining the control configuration (left columns of Figure 28,

Figure 29 and Figure 30) we see varying diversity in the profiles given by the four methods. The largest differences are seen for m03. The smallest differences are seen for m02 and m06.

Examining the differences in the profiles given by method 1 and 2 indicates the impact of using the mesoscale model variables to give Monin-Obukhov length (method 1) instead of a prescribed value (method 2). For m02, the profiles given by method 1 and 2 are very nearly the same. For m03, method 1 profile gives lower winds than method 2. For all other stations method 1 gives higher winds than method 2.

For m03, the mesoscale evaluated Monin-Obukhov lengths correspond to unstable conditions. Whilst for the other stations the mesoscale evaluated Monin-Obukhov lengths are evaluated as mainly stable. The reason for this may be that, generally, the large-scale forcing given by the wind class profiles are stable. For m03, however, some properties relating to its position in the terrain give rise to an unstable profile. This may be related to predominant upslope flow associated with a cooling of air as it ascends, resulting in cooler air flowing above a warmer surface.

Method 2 and 3 both assume neutral conditions in the mesoscale model boundary layer, thus they follow rather parallel profiles in the figures. However there profiles are not coinciding because in method 1 friction velocity is the mesoscale output used, while for method 2 it is the wind speed interpolated at 50 m. The differences in methods 2 and 3 therefore also illuminate the departure of the mesoscale winds to the neutral log profile. In most cases, method 2 gives lower wind profile relative to the method 3 profiles. This again indicates a tendency for the mesoscale model boundary layer to be slightly stable. However, this is not seen for m03 where, this time, a more neutral boundary layer is suggested. One complicating issue in the comparison of method 2 and 3 is that the topography corrections are applied in different ways. Differences or similarities in the method may thus incorporate effects of differences in the topography correction in addition to the considerations to boundary layer stability.

Method 3 uses the model winds interpolated to 50 m only, whereas method 4 uses model winds interpolated to 10, 25, 50, 100, and 200 m. We expect method 3 and 4 to agree at 50 m, but the differences above and below 50 m indicate how the mesoscale model profile departs from the standard WAsP profile. In most cases the differences in method 3 and 4 are small, suggesting the WAsP stability correction accords with the mesoscale boundary layer profiles. However for m07, m08, m09, method 4 suggests a more stable profile than method 3. Moreover, for m03, method 4 suggests more unstable profiles than method 3, in harmony with what was found for m03 when examining the other methods.

Now we examine the profiles given by the two other mesoscale model configurations. First, we examine the configuration where the land surface temperature is increased, and the sea surface temperature is decreased, relative to the lowest model level air temperature at initial time. The profiles are given in the centre column of Figure 28,

Figure 29 and Figure 30. As expected there are now large differences in the profile calculated using method 1 and 2. For a given geostrophic wind, unstable conditions lead to a higher friction velocity relative to neutral conditions. Therefore, for the same friction velocity, when neutral conditions are assumed, the geostrophic wind will be overestimated compared to adjustment to unstable conditions in the geostrophic drag law. This is the reason why method 2 always gives profiles with higher wind than the profiles given by method 1. It should be noted that the same WAsP default stability correction is applied to all cases. The correction is not adjusted to the new more unstable boundary layer conditions, hence it can be expected that method 1 has a serious underestimate of the surface winds.

Comparing methods 3 and 4 we see that, since the stability correction does not reflect the new surface temperature conditions, there are large differences in the profiles. Method 4 gives profiles showing reduced shear, as expected for unstable conditions. Agreement of the profiles at 50 m is because method 3 uses 50 m interpolated winds as the basis of the profiles. Interestingly, the wind profile from method 2 and 4 often agree at 10 m.

Next, we examine the configuration where the land surface temperature is decreased, and the sea surface temperature is increased, relative to the lowest model level air temperature at initial time. The profiles are given in the right column of Figure 28,

Figure 29 and Figure 30. There are large differences in the profile calculated using method 1 and 2. For a given geostophic wind, stable conditions lead to a lower friction velocity, relative to neutral conditions. Therefore, for the same friction velocity, when neutral conditions are assumed, the geostrophic wind will be underestimated compared to adjustment to stable conditions in the geostrophic drag law. This is the reason that method 2 always gives profiles with lower wind than the profiles given by method 1. It should be noted again that the same WAsP default stability correction is applied. The correction is not adjusted to the new more stable boundary layer conditions, hence it can be expected that method 1 has a serious overestimate of the surface winds.

Comparing methods 3 and 4 we see that once again, since the stability correction does not reflect the new surface temperature conditions, there are large differences in the profiles. Method 4 gives profiles showing increased shear, as expected for stable conditions. Agreement of the profiles at 50 m is because method 3 uses 50 m interpolated winds as the basis of the profiles. Interestingly the wind profile from method 2 and 4 are often approaching agreement at 10 m.

# 11 Verification

In this section a comparison of the generalized wind climates generated by the numerical wind atlas method (KAMM/WAsP) is made with the generalized wind climates derived from the measurement data at each of the measurement stations Mortensen et al (2010). The sites for the measurement station are shown in Figure 31.

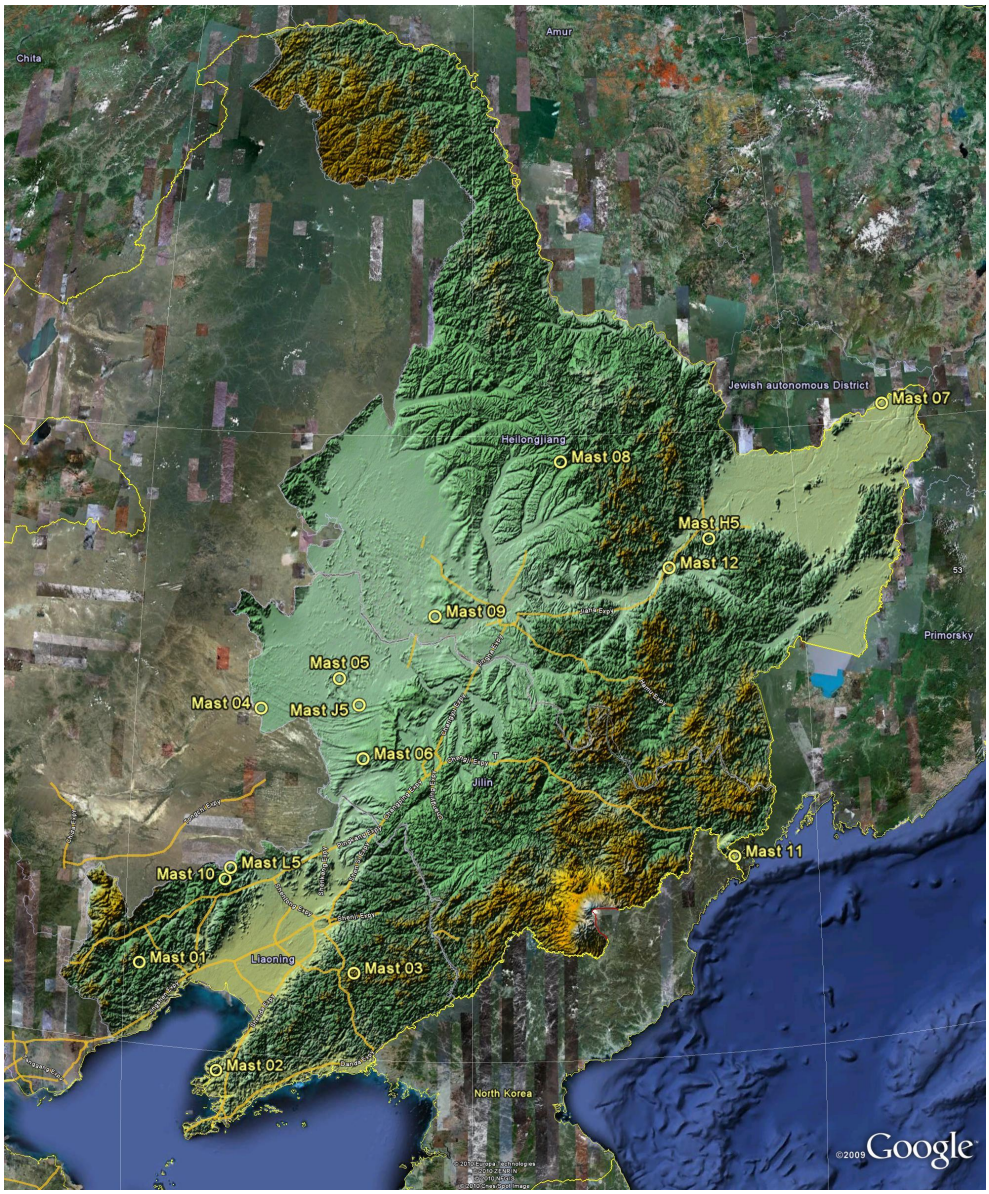


*Figure 31: Overview map of Dongbei showing the location of the 15 meteorological masts erected as part of the measurement project. Stations m01, m02, m03, m04, m05, m06, m07, m08, and m09, were used in the verification (Image © 2010 Europa Technologies, NFGIS, ZENRIN, US Dept. of State Geographer and Google Inc.). Source: Mortensen et al (2010).*

The verification is given in two parts, i. verification of annual mean generalized wind speed, and ii. verification of wind speed and direction distributions.

**Verification of annual mean wind speed**

Table 4 gives a summary of the 50 m generalized wind speed verification for stations m01, m02, m03, m04, m05, m06, m07, m08, and m09, using data for the complete year 2009. The verification is made for the generalized winds for standard conditions (i.e. flat terrain) with 0.03 m surface roughness. The numerical wind atlas generalized winds are calculated for 2009 by using wind class weightings based on the reanalysis data for 2009 only. The mesoscale configuration giving the minimum error for each station is shown in Table 4. In most cases this was the cooler-land / warmer-sea configuration, except for m01 and m03.

*Table 4: The verification of the annual mean generalized wind speed for 2009 at 50 m over flat homogeneous terrain with roughness of 3 cm. OWA is observed wind atlas wind speed [m/s] and NWA is numerical wind atlas wind speed [m/s]. The model configuration is given in the last column.*

| | wind speed z=50m z_0=0.03m | | | |
|---|---|---|---|---|
| Mast | OWA | NWA | Error [%] | Configuration |
| m01 | 4.70 | 4.88 | 3.83 | NS105_10 |
| m02 | 6.81 | 5.66 | -16.89 | NSb05_10 |
| m03 | 5.51 | 6.22 | 12.89 | NS105_20 |
| m04 | 6.78 | 6.32 | -6.78 | NCb05_10 |
| m05 | 6.74 | 6.37 | -5.49 | NCb05_10 |
| m06 | 6.72 | 6.41 | -4.61 | NCb05_10 |
| m07 | 6.01 | 6.27 | 4.33 | NNb05_10 |
| m08 | 5.60 | 6.20 | 10.71 | NNb05_10 |
| m09 | 6.83 | 6.20 | -9.22 | NNb05_10 |

| | |
|---|---|
| mean error | -1.25 |
| mean absolute error | 8.31 |

**Verification of wind speed and direction distributions**

Next the generalized wind speed and direction distributions are presented derived from observations and from the numerical modelling. Figure 32, Figure 33, and Figure 34 show the generalized wind direction and distributions derived from the mesoscale modelling against those derived from measurements at stations m01, m02, m03, m04, m05, m06, m07, m08, and m09. The standardized conditions are for height of 50 m and flat terrain with homogeneous roughness of 3 cm.

The wind roses show the frequency of each wind direction sector, i.e. which wind directions are most common, irrespective of wind speed. The fainter lines in the wind speed distribution graphs show the wind speed distribution for each sector. These distributions are based on Weibull distributions fitted for each direction sector. The bold line is the sum of the sectorwise distributions, i.e. the wind speed distribution irrespective of wind direction. The dashed line is the Weibull fit using the wind speed distribution for all sectors.

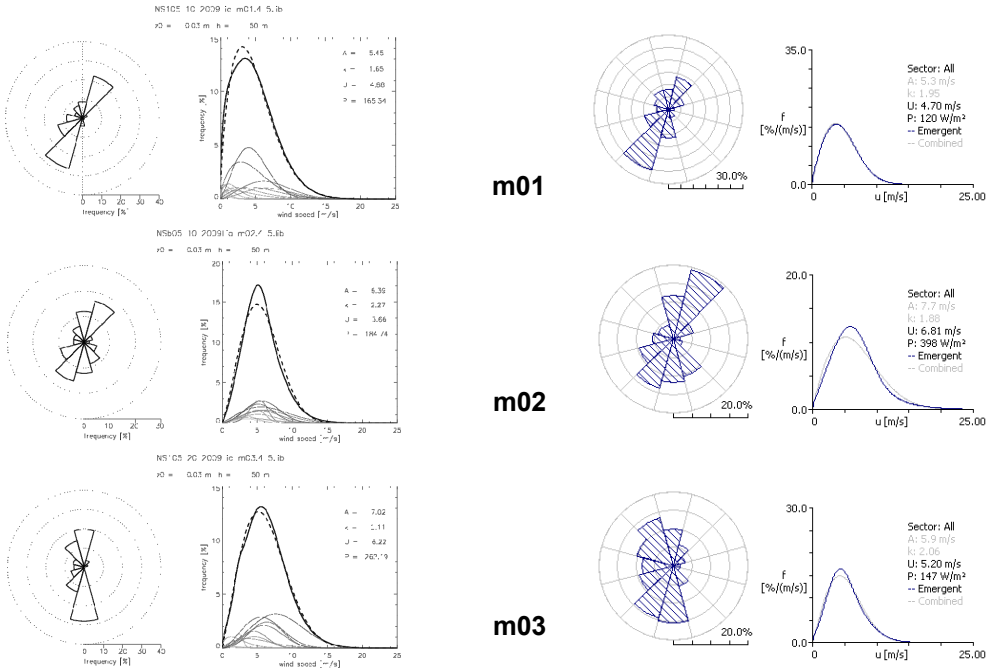


*Figure 32: Generalized wind direction and speed distributions derived from modelling (left side) and derived from measurements (right side). The height is 50 m and roughness is 3cm for stations m01, m02, and m03.*

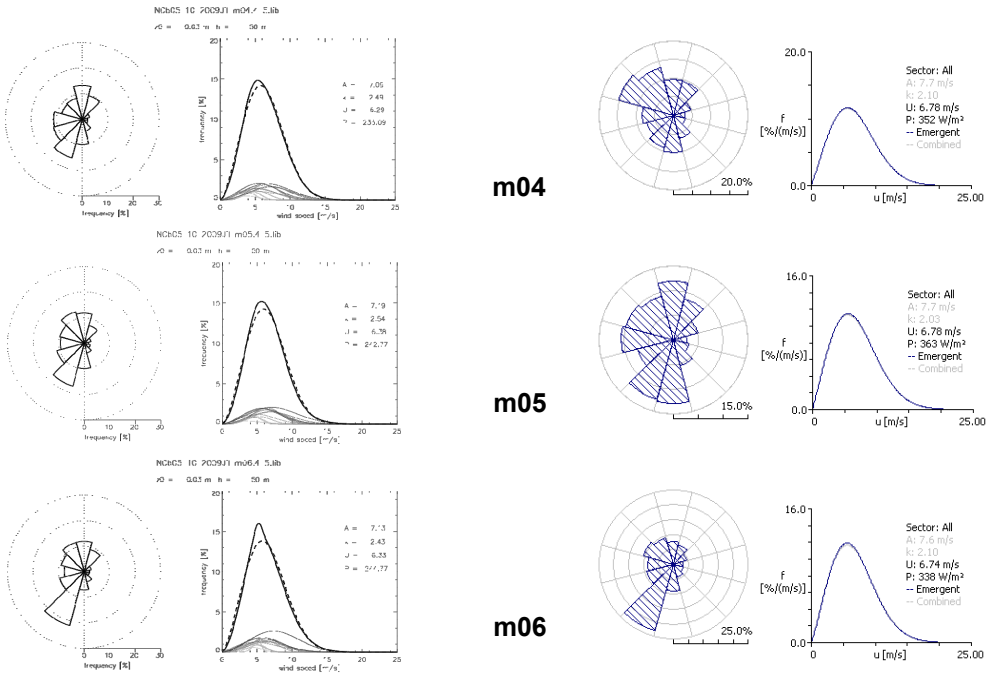


*Figure 33: Generalized wind direction and speed distributions derived from modelling (left side) and derived from measurements (right side). The height is 50 m and roughness is 3cm for stations m04, m05, and m06.*

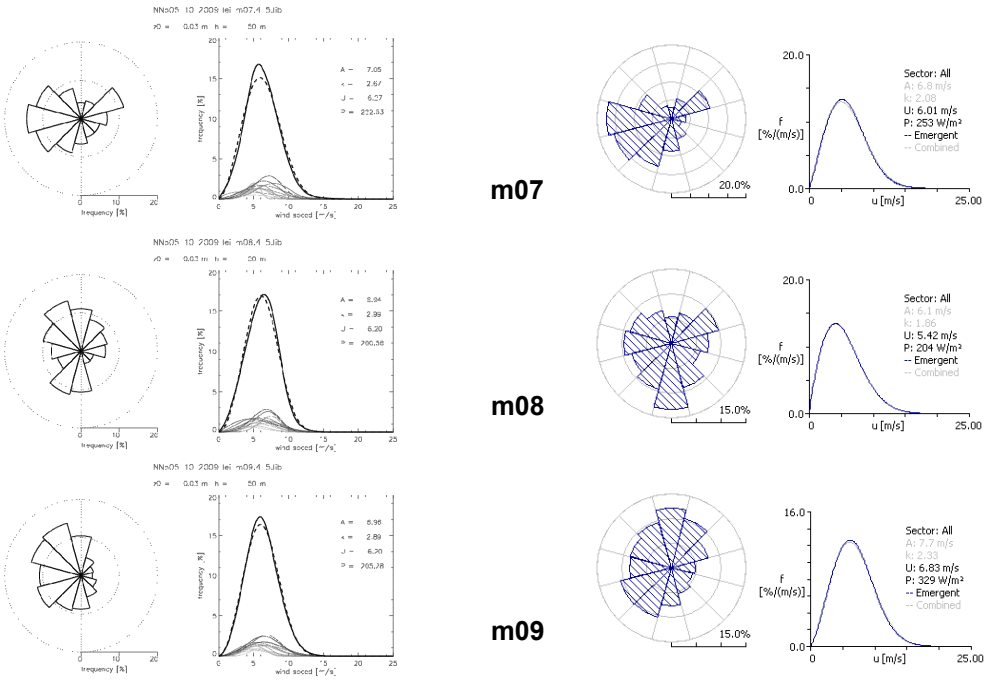


*Figure 34: Generalized wind direction and speed distributions derived from modelling (left side) and derived from measurements (right side). The height is 50 m and roughness is 3cm for stations m07, m08, and m09.*

**Summary**

Overall the qualitative agreement of the modelling and measured results is good. From Figure 32, Figure 33, and Figure 34 we see that in most cases the direction distributions are in good agreement. Only m04 and m08 show some disagreement in the predominant wind direction sectors. The mesoscale modelling in terms of agreement of mean wind speed gives a performance that is comparable to that found in other studies (Frank, 2001 and Mortensen et al, 2005). Using the best modelling configuration for each station gives a mean error of -1.25% (slight negative bias) and a mean absolute error for the 9 stations of 8%. If we use just a single mesoscale model configuration for the entire region of interest the mean error is -4% and mean absolute error is 13% . This indicates that the region has a diversity of climate conditions. Further improvement of the wind resource modelling by KAMM/WAsP may be achieved through more specific configurations for small domains, as was performed from the Wind Atlas for Egypt study (Mortensen et al, 2005).

The mean wind speed agreement is poorest for station m02. However for m02 a good agreement in the direction distributions was indicated (see Figure 32). A similar behaviour is seen for m03, in which the wind direction distributions is captured fairly well but the mean wind speed is overestimated. For m08, however wind direction and mean wind speed together are more poorly captured. The stations with better than average agreement between modelled and measured wind resource were m01, m04, m05, m06, and m07. The stations with worse than average agreement were m02, m03, m08, and m09. From Figure 31 we can see that m04, m05, m06 and m07 are in rather simple terrain settings, whereas m01 appears to be in more complex terrain. Station m03 and m08, are in more complex terrain settings, whereas m02 is in relative complex terrain and in a coastal region. Station m09 appears to have the least complex setting of all the stations with worse than average agreement. On the whole the verification findings are in

line with what was found in the sensitivity tests described in Section 7. The next section looks deeper into quantifying station terrain setting complexity.

# 12 Mesoscale surface roughness and orography – terrain complexity and its indication for model validation

Several indices are used to describe the complexity of the mesoscale topography. The normalized roughness length (z0) and elevation (h) are calculated as the standard deviation of z0 and h deviated by the mean of them (σ(z0)/<z0> and σ(h)/<h>) over areas of 3 by 3, 5 by 5, 11 by 11 and 21 by 21 grid points. Over an area of 11 by 11 grid points, Figure 35 shows that there is an indication the error is larger in complex terrains where the roughness length and elevation variation is larger. The scatter is large. Note, other sources of uncertainties are not considered here (for instance, the elevation of m03 and m08 are well above 1000 mb which is first level of four used for wind classification).

It's planed to examine the directional variability of the surface elevation and roughness. In connection with the wind classification, the number of sectors is expected to be optimal if it describes well the actual distribution of the surface conditions. Too few sectors in complex terrains are expected to give larger uncertainty.

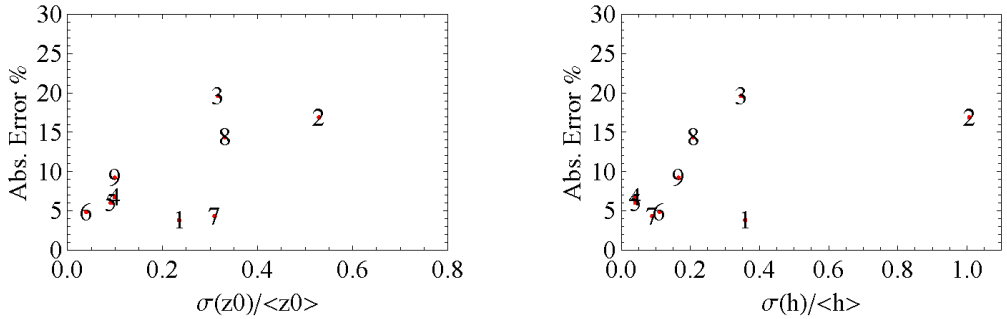


*Figure 35: Absolute error (%) of KAMM/WAsP generalized wind (50 m and 0.03 m roughness) at 9 masts (marked with numbers 1-9) as a function of the normalized roughness length (left) and normalized elevation (right) over an area of 11 by 11 grid points, approximately 50 km by 50 km.*

# 13 Comparison of CMA and Risø DTU results

In this section the suggested form of comparison is to attempt to verify the CMA wind atlas results (Zhu et al, 2010) with the station measurements in the same manner as that the comparison is made for the Risø DTU wind atlas results. This is the first time that a method of verification using generalized winds from the WRF mesoscale model has been performed.

**Verification of WERAS**

In order to verify CMA's WERAS results it was necessary to attempt to remove the effects of the mesoscale resolved terrain on the wind climate. This means the removal of orographic speed-up effects and roughness change effects, at the resolution of the mesoscale model (5km). This was done using the WAsP software. First WAsP maps were created for the terrain, as it is obtained from the WRF pre-processing system (WPS), for each of the three domains used by CMA. These maps are shown in Figure 36.

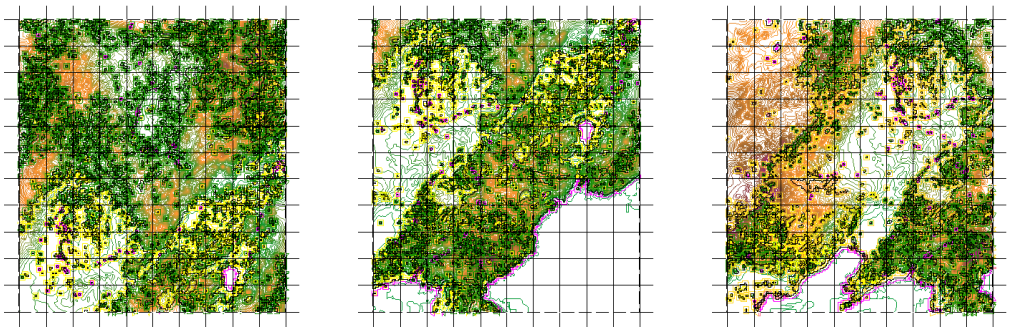

*Figure 36: WAsP maps prepared for the three WRF modelling domains used by CMA. Single line contours represent elevation and double line contour represent roughness changes. The elevation and roughness length information was provided by CMA.*

Next CMA created files containing the simulated winds at the locations of the stations. These files represent the simulated climate at the stations. As CMA use a statistical downscaling methodology, consideration had to be given to the weighting of each of the simulations. The simulated climate data was then imported into the WAsP software, and making use of the maps of the WRF terrain, the simulated climates were generalized, i.e. wind climate given for standard conditions. The generalized winds derived from WRF simulations and the generalized winds derived from measurements are given in Table 5.

It can be seen that generalized winds from modelling and measurements are in very good agreement for m04, m05, m06. These stations are in relative simple and homogeneous terrain. On the other hand for m01, m03, m07 and m08 the agreement is poorer (>20% differences). Overall the mean error is 11%, a positive bias, and the mean absolute error is 14%.

An interesting comparison can be made using the simulated wind climate directly against the measured wind climate at 50 m. In these cases, no allowance for the impact of

orographic speed-up or roughness changes are made to the measurements or the simulated winds. The comparison is shown in Table 6. Rather surprisingly the mean error is now only 3% and the mean absolute error is 10%. This is better than the comparison of the generalized wind climates.

This surprising result suggests that either the manner in which the generalized wind climate is made for WRF is sub-optimal or that the direct comparison gives a better agreement by chance. One would expect that an optimal generalization procedure would increase the agreement between modelling and measurement. At this stage it is suspected that the generalization method used for KAMM may need further adaptations for it to work well with WRF. Section 14 examines the difference in the wave-number spectra for the KAMM and WRF results. Somewhat smoother wind fields are produced by the WRF simulations, suggesting that using the KAMM generalization procedure on WRF results may over compensate for orographic speed-up and roughness change effects, thereby actually introducing errors to the results.

*Table 5: The verification of the annual mean generalized wind speed at 50 m over flat homogeneous terrain with roughness of 3 cm. OWA is observed wind atlas wind speed [m/s] and NWA is numerical wind atlas wind speed [m/s].*

| | wind speed z=50m z_0=0.03m | | |
|---|---|---|---|
| Mast | OWA | NWA | Error [%] |
| m01 | 4.70 | 6.84 | 45.53 |
| m02 | 6.81 | 6.68 | -1.91 |
| m03 | 5.51 | 6.86 | 24.50 |
| m04 | 6.78 | 6.84 | 0.88 |
| m05 | 6.74 | 6.57 | -2.52 |
| m06 | 6.72 | 6.87 | 2.23 |
| m07 | 6.01 | 7.26 | 20.80 |
| m08 | 5.60 | 6.65 | 18.75 |
| m09 | 6.83 | 6.38 | -6.59 |
| | mean error | | 11.30 |
| | mean absolute error | | 13.75 |

*Table 6: The verification of the annual mean wind speed at 50 m. Obs is **obs**erved wind wind speed [m/s] and Num is **num**erical wind atlas wind speed [m/s].*

| | wind speed z=50m | | |
|---|---|---|---|
| Mast | Obs | Num | Error [%] |
| m01 | 4.98 | 6.30 | 26.51 |
| m02 | 7.24 | 6.41 | -11.46 |
| m03 | 6.72 | 6.80 | 1.19 |
| m04 | 6.51 | 6.42 | -1.38 |
| m05 | 6.42 | 6.16 | -4.05 |
| m06 | 5.94 | 6.44 | 8.42 |
| m07 | 6.05 | 5.30 | -12.40 |
| m08 | 4.01 | 4.68 | 16.71 |
| m09 | 5.74 | 5.99 | 4.36 |
| | mean error | | 3.10 |
| | mean absolute error | | 9.61 |

# 14 Spectral analysis

The wave-number spectra of energy density from KAMM/WAsP are examined for the three domains (north:NN, centre:NC, south:NS), for the wind resource maps (WRM) as well as wind assessment maps (WAM), see Figure 37. The results are similar, whereas in NS it can be seen that the energy level is slightly lower for WAM for lower wave numbers. In Figure 37, the blue dots are the mean spectrum for all west-east transects and the green dots are the mean spectrum for all north-south transects. In NC and NS, the north-south direction has more wind variation than the west-east direction.

The mean wind speed of WRM from CMA WRF output is analyzed similarly and the spectra are presented in Figure 38. The simulations from KAMM and WRF are both 5 km resolution. The striking differences between Figure 37 and Figure 38 are:

i. KAMM spectra have flat slopes, very likely because of the unified large scale forcing, thus energy is transferred to smaller scales in a way different from that provided by a weather model, e.g. WRF in real mode. On the other hand, although in NS the spectra from WRF outputs are also a bit flat (Figure 38), the slope in $k<2\ 10^{-4}$ rad./m (~ 31 km) is as expected.

ii. KAMM spectral energy density drops at a scale approximately 15 km, while WRF spectral energy density fades at a scale of about 30 km. This suggests that, for KAMM, the wind variation is not resolved for scales smaller than 15 km, while for WRF, the wind variation is not resolved for scales smaller than 30 km.

The KAMM/WAsP method uses spatially uniform geostrophic winds to force the mesoscale model, so little variance would be expected to be at scales larger than the dominant scales of the topography. However, the separate wind class simulations are weighted as a function of geographic position within the domain. Therefore, we would expect variance to be added at the scales of the reanalysis dataset. However, there will still be missing variance in the scales between the reanalysis dataset and the dominant scales of the topography. The impact of this on wind resource mapping may be a hypothetical minimum error limit or uncertainty implicit in the KAMM/WAsP methodology.

Concerning the spectra for the WRF simulations; the flattening out of the variance at smaller wave-numbers may be an indication of insufficient spin-up of the model, or too large differences in the grid resolutions of the dataset used to provide boundary conditions and subsequent nested domains. CMA used two nested domains at 25 km and 5 km resolution. It would be interesting to examine the spectra for a WRF set-up that used a third outer domain, at 45 km resolution.

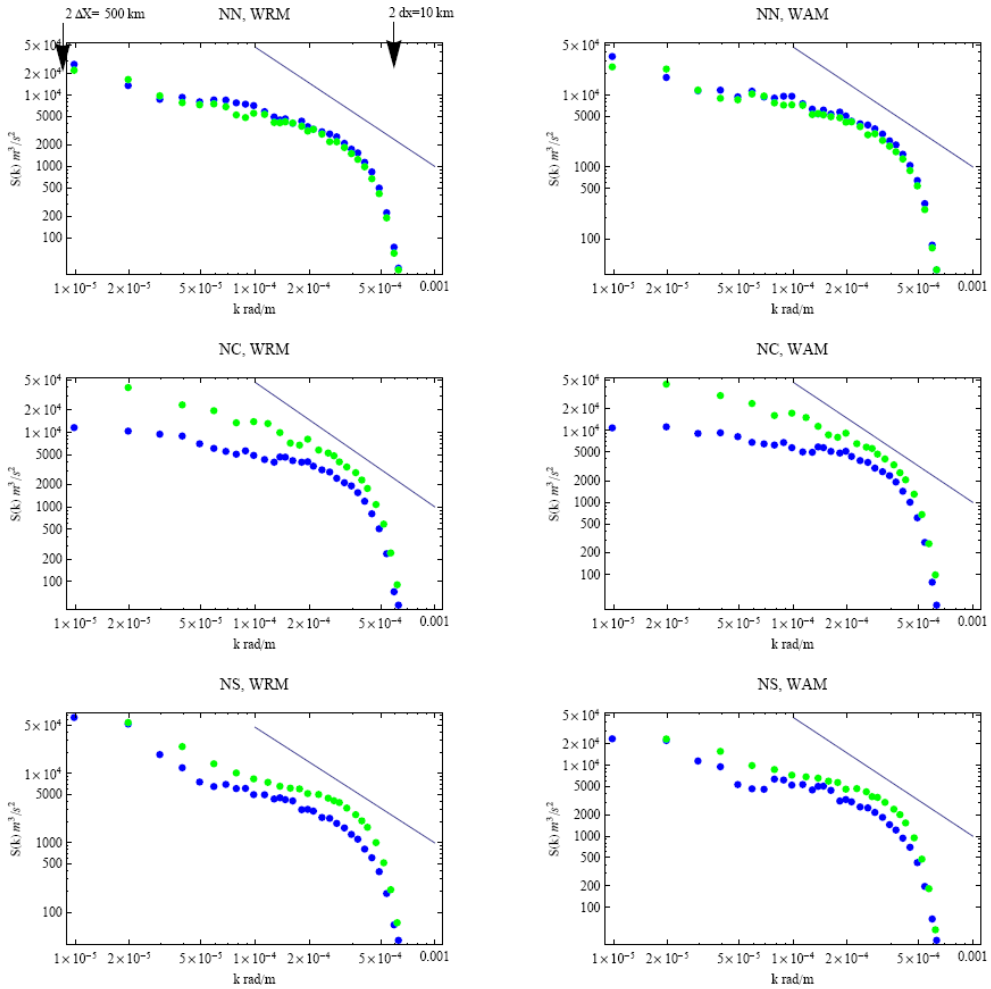


*Figure 37: Spatial spectral energy density of wind speed as functions of wave number k, for three domains (north-NN, center-NC, south-NS). Blue dots show the mean of all east-north transects and green dots show the mean of all north-south transects. Left column is based on wind resource map (WRM), right column is based on wind assessment map (WAM). Data are from KAMM/WAsP simulations. The solid line indicates a slope of -5/3. The arrows labelled 2ΔX and 2Δx, in the top-left plot, indicate wave-numbers for the reanalysis and mesoscale resolutions, respectively.*

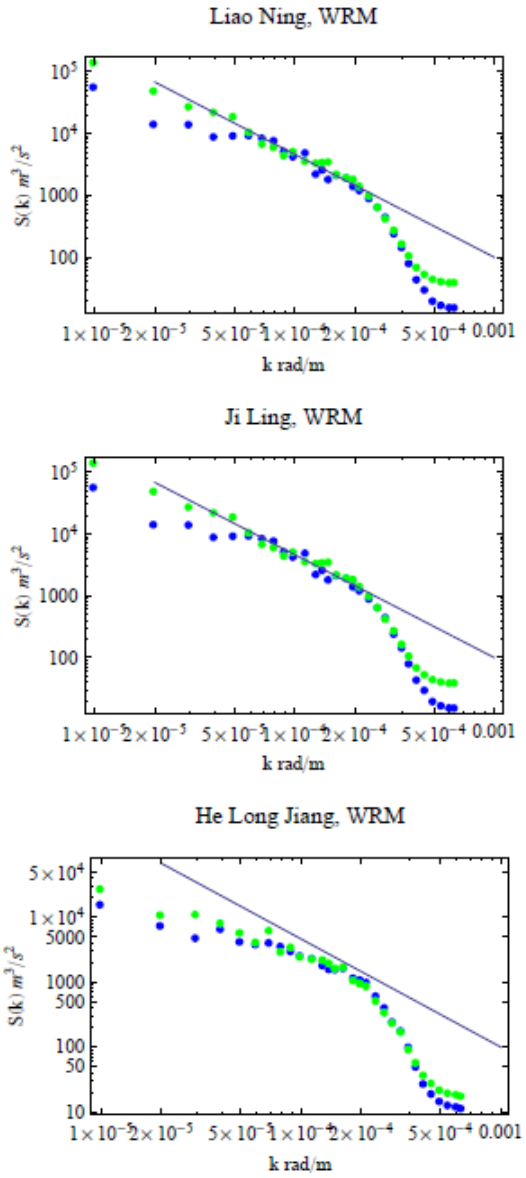


*Figure 38: Similar to left column in Figure 37, with the blue dots as the mean of all west-east transects and the green dots as the mean of all north-south transects. Here the data are from CMA's WERAS method using the selective downscaling method and WRF.*

# 15 Comparison of KAMM and WRF for Harbin test area

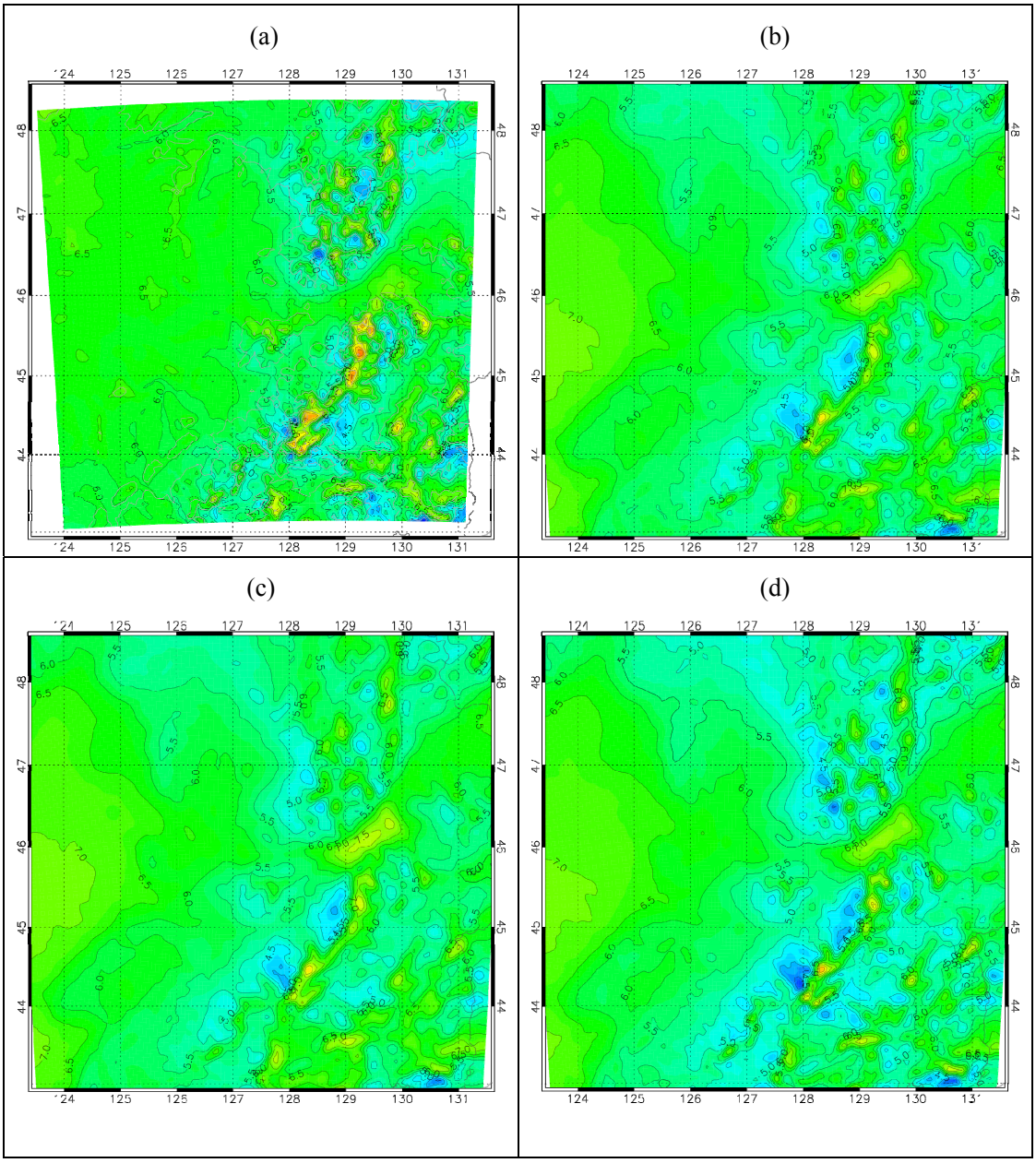


*Figure 39: Comparison of mean wind speed for the Harbin test area: annual mean simulated wind speed at 100 m given by (a) KAMM model, (b) WRF model, (c) WRF model with a smoothed topography and (d) WRF model with no surface heat fluxes.*

The WRF mesoscale model was run by CMA in 'real' mode (Zhu el al, 2010) , meaning that initial conditions and boundary conditions for the model represented actual meteorological situations that have or may occur. WRF can also be run in 'idealized' model, which is rather like the way that the KAMM model is run, in that the meteorological situation simulated is not representing a past or forecast meteorological situation but rather a condition generated for experimental, flow evaluation or research purposes. WRF was run using the same wind class set (121 wind classes) that was used in KAMM for the Harbin test area, see Section 8. The results of the comparison are shown in Figure 39.

Qualitatively, the wind climate given by WRF looks similar to a rather smoothed version of wind climate given by KAMM. In the plain in the western portion of the domain, the resources are similar. However in the higher terrain there is a greater variation of the resource in KAMM compared to WRF. On the other hand in the gap, WRF displays a ~20% higher wind speed than KAMM. For the WRF simulations where topography is smoother slightly higher winds are simulated through the gap. For the WRF simulations where the surface heat fluxes are disabled slightly lower winds are simulated through the gap. There is also slightly more variation of resource in the elevated terrain regions. This suggests more stable conditions.

# 16 Conclusions

The KAMM/WAsP method generated wind resource maps and datasets for the 3 Dongbei provinces. Verification has been carried out for KAMM/WAsP using measurement data from 9 of the project masts. A mean absolute error of 8% is evaluated. Verification has been carried out for CMA's WRF using WAsP and WAsP maps of the WRF domains. A mean absolute error of 14 % is evaluated. For direct comparison of WRF to measurements a mean absolute error of 10 % is evaluated. This is considered surprising as no microscale effects are present in WRF, and is indicative that the generalization procedure needs further adaptation for use with WRF output.

Spatial spectral analysis of wind resources suggests that, for KAMM, the wind variation is not resolved for scales smaller than 15 km, while for WRF, the wind variation is not resolved for scales smaller than 30 km. Wind resource calculated using WRF in idealized mode using KAMM/WAsP wind classes as forcing reinforce the finding that the WRF results appear to be smoother. This may be associated with treatment of the staggered grid used in WRF at the post-processing stage or strong diffusion used in the model equations, in order to help maintain model stability for operational purposes. Another very interesting aspect of the spectral analysis is that it may illuminate a hypothetical minimum error limit expected for a given model and given methodology. If the spectra show there is missing variance, then this will likely have implications on the wind resource results obtained.

Multiple sensitivity tests have been carried out for the whole of the numerical wind atlas methodology (from the determination of the geostrophic wind and the appropriate temporal sampling needed for wind/weather classification, to consideration of how mesoscale modelling is fed to microscale models, i.e. wind generalization). The results assist in the assessment of sources of error, and it is expected soon to provide input for mapping uncertainty estimates. Results indicate larger uncertainty and error in the mountain/hill terrain and/or coastal regions. This is reinforced in the results of the verification and an indexing of the mesoscale terrain complexity in relation to numerical wind atlas error. In areas where sensitivity and uncertainty is high a joint campaign of more specific modelling (using higher resolution and specific surface temperature configuration) and wind measurement is recommended.

Further studies are required to relate more generally the sensitivity analysis of the numerical wind atlas methodology to the uncertainties in the resulting wind resource data. Uncertainty estimation for all locations within the mapped area is now a step closer to realization after the development of indexing of the mesoscale terrain complexity presented in this report. It would be of great value as it helps the user of the modelled data to assess to what extent further measurement campaigns are required in a given area.

It should be remembered that only one year of measurement data is used for the model verification. When the verification period is shortened we normally expect an increase in the uncertainty, therefore further measurements at current sites and additional sites would be of great value for verification. Multi-year measurements would allow for an assessment of uncertainty for single year mean wind statistics. More measurement sites

would not only allow verification of modelled wind resources but also importantly would provide much needed data for verification of uncertainty estimation.

The mesoscale project has not only generated a number of wind resource products, from both CMA and Risø DTU, but it has also involved many new investigations into aspects of mesoscale modelling in the numerical wind atlas frame work. The project has created a good research relationship between the mesoscale modellers at CMA and Risø DTU, with great openness towards sharing knowledge, methods and results. After the project is complete it is hoped that collaboration will continue to flourish.

# 17 Acknowledgements

The Risø DTU authors would like to especially thank Zhu Rong for her collaborative spirit in this project, for her very large contribution in the twinning process thereby making the mesoscale project a success, and her ability to trigger many fruitful discussions on numerical wind atlas methodologies. Yuan Chunhong, He Xiaofeng, Zhou Rongwei, Gong Qiang are thanked for their large contributions to the mesoscale project. Finally Yang Zhinbin is thanked for his coordination and warm hospitality. On the Risø DTU side, Niels Gylling Mortensen and Jens Carsten Hansen are thanked for coordination, providing data for verification, feedback on application of numerical wind atlas data and many inputs through discussions on all aspects of the methodologies.

# 18 References

Adrian, G., F. Fiedler, 1991: Simulation of unstationary wind and temperature fields over complex terrain and comparison with observations. Beitr. Phys. Atmosph., 64:27-48

Adrian, G, 1994. Zur Dynamik des Windfeldes über orographisch gegliedertem Gelände, Ber Deutschen Wettedienstes 188, Offenbach am Main 1994, 142 pp.

Frank, H. P., L. Landberg, 1997. Modelling the wind climate of Ireland. Boundary-Layer Meteorology, 85:359-378

Frey-Buness, F., D. Heimann, R. Sausen, 1995. A statistical-dynamical downscaling procedure for global climate simulations. Theor. Appl. Climatol., 50:117-131

Kalnay E, Kanamitsou M, Kistler R, Collins W, Deaven D, Gandin L, Irebell M, Saha S, White G, Woollen J, Zhu Y, Leetmaa A, Reynolds R, Chelliah M, Ebisuzaki W, Huggins W, Janowiak J, Mo KC, Ropelewski C, Wang J, Jenne R, Joseph D, 1996. The NCEP/NCAR 40-year reanalysis project. Bulletin of the American Meteorological Society **77**: 437-471

Klemp, J.B., D.R. Durran, 1983. An upper boundary condition permitting internal gravity wave radiation in numerical mesoscale models. Mon. Wea. Rev. 1983, 111, 430-444.

Mortensen, N.G., J.C. Hansen, J. Badger, B.H. Jørgensen, C.B. Hasager, L. Georgy Youssef, U. Said Said, A. Abd El-Salam Moussa, M. Akmal Mahmoud, A. El Sayed Yousef, A. Mahmoud Awad, M. Abd-El Raheem Ahmed, M. A.M. Sayed, M. Hussein Korany, M. Abd-El Baky Tarad, 2005. Wind Atlas for Egypt, Measurements and Modelling 1991-2005. New and Renewable Energy Authority, Egyptian Meteorological Authority and Risø National Laboratory. ISBN 87-550-3493-4. 258 pp.

Mortensen, N.G., Z. Yang, J.C. Hansen and O. Rathmann, 2010. Meso- and Micro-scale Modelling in China: Wind atlas analysis for 12 meteorological stations in NE China (Dongbei). Risø-I-3072(EN).

Troen, I., E. L. Petersen, 1989. European Wind Atlas. Risø National Laboratory for the Commission of the European Communities, Roskilde, Denmark, ISBN 87-550-1482-8.

Zhu Rong, He Xiaofeng, Zhou Rongwei, Yuan Chunhong, Gong Qiang, 2010. A01 WERAS/CMA Modelling in NE China. Project report for Sino-Danish Wind Energy Development Programme(WED) "Mesoscale and Microscale Modelling in NE China"

# 19 Appendix A – additional figures

Figures of simulated wind climates and generalized wind climate at levels not included in the main text.

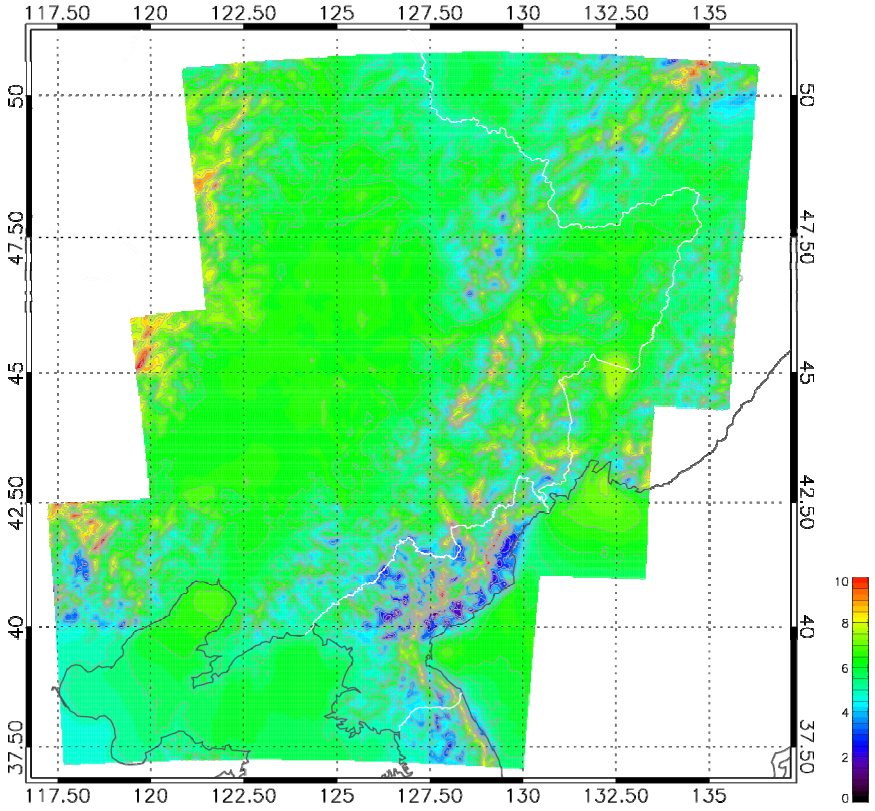


*Figure 40: Mean simulated wind speed at 70 m. The contour interval is 0.5 m/s.*

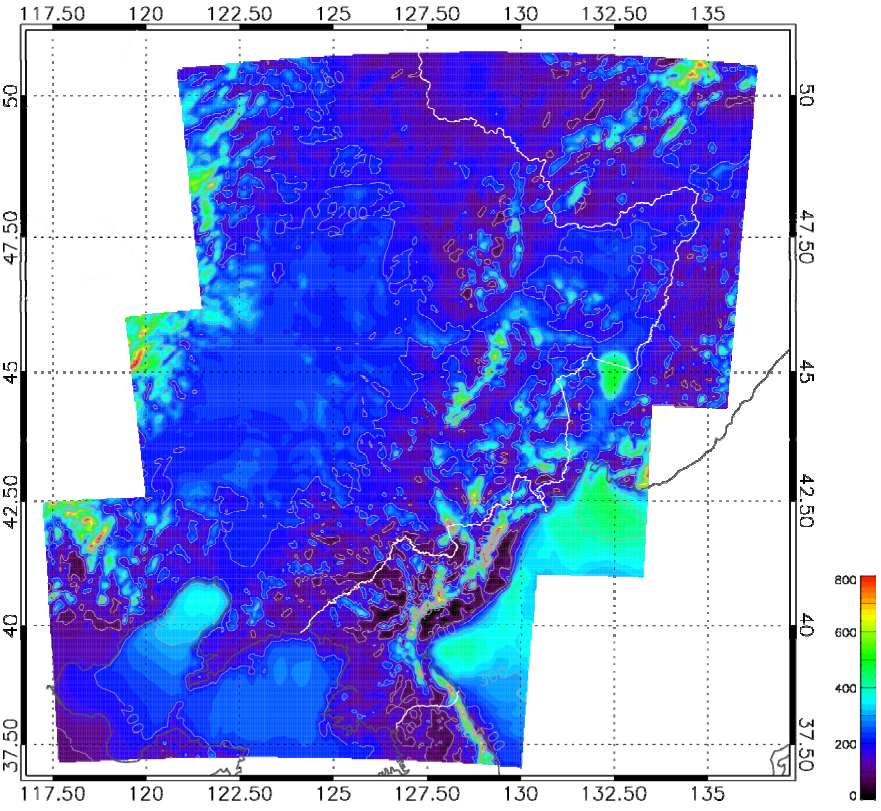


*Figure 41: Mean simulated wind power density at 70 m. The contour interval is 100 W/m$^2$.*

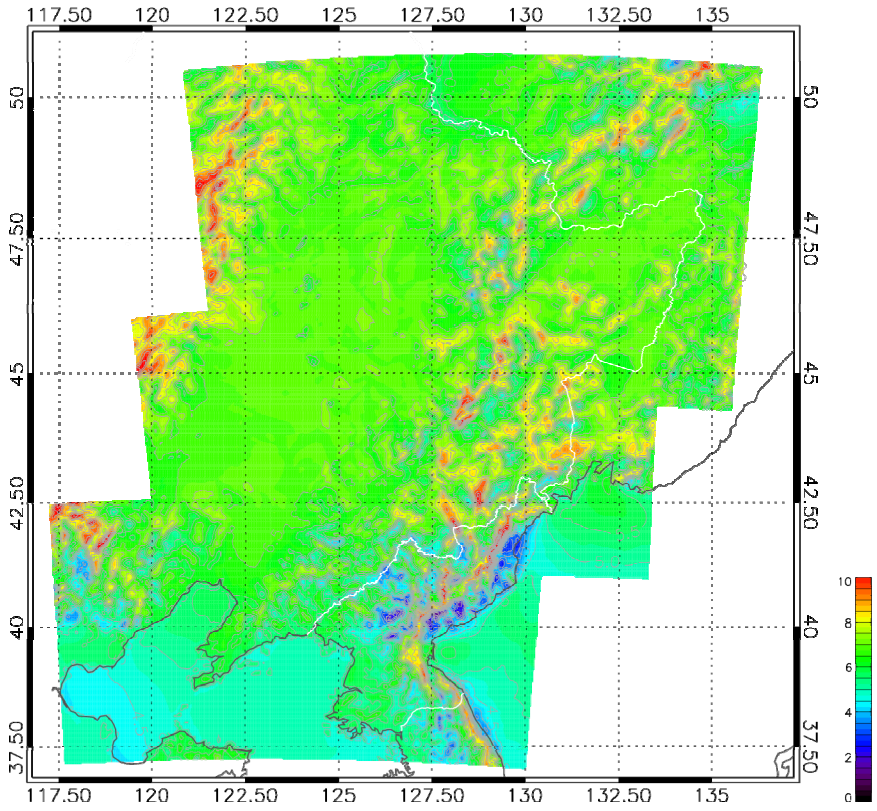


*Figure 42: Mean generalized wind speed at 50 m a.g.l. for 0.03 m roughness. The contour interval is 0.5 m/s.*

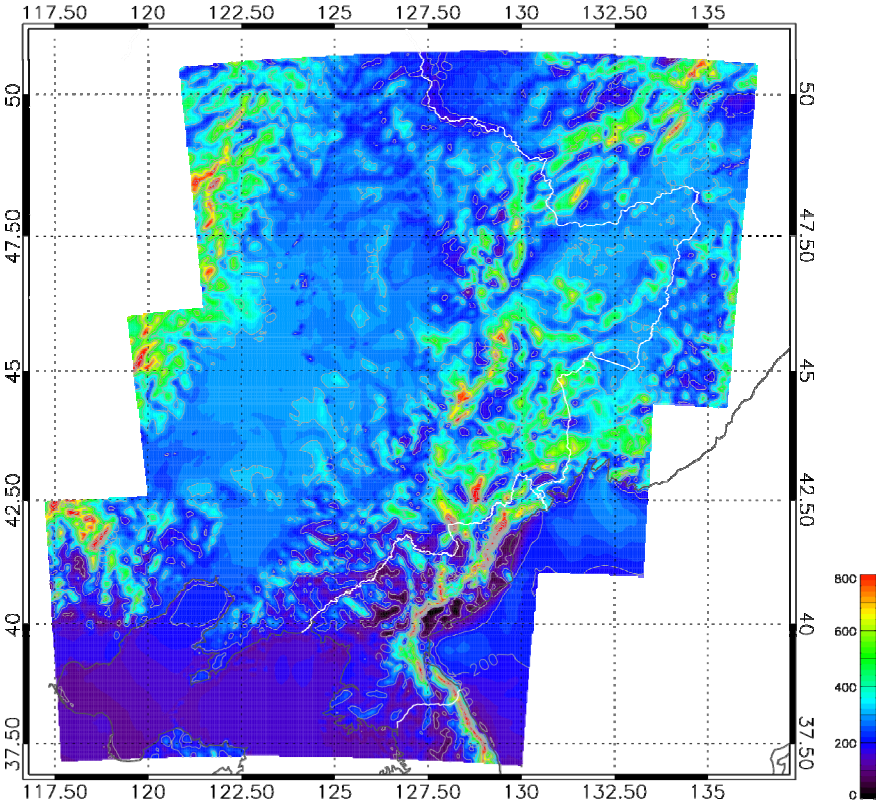


*Figure 43: Mean generalized wind power density at 70 m a.g.l. for 0.03 m roughness. The contour interval is 100 W/m2.*

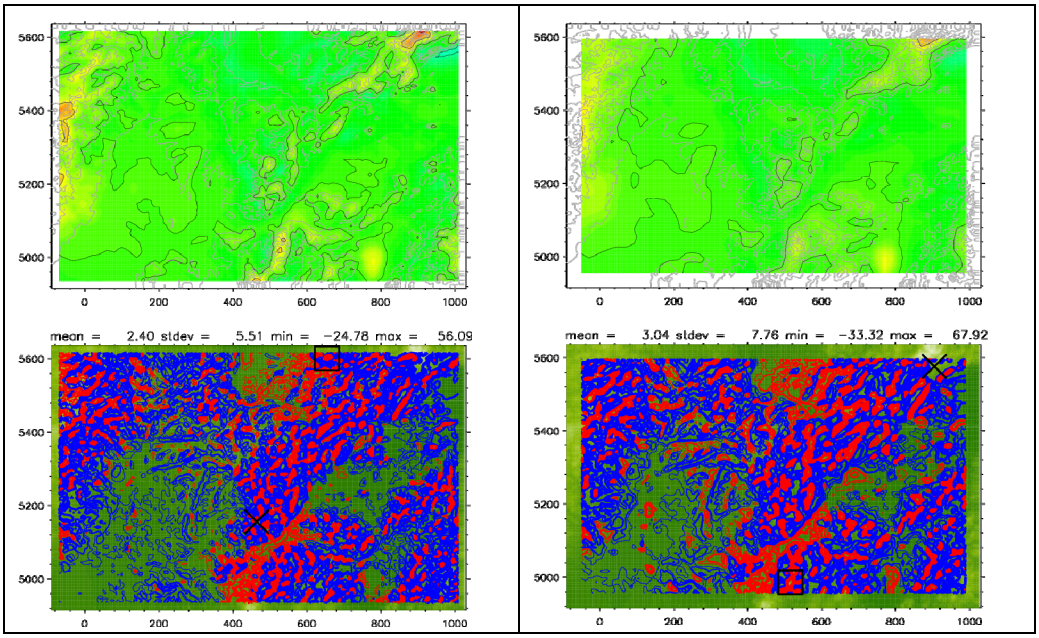


*Figure 44: Maps of mean simulated wind speed at 100 m (upper panels) for 10 km (left) and 20 km (right) resolution mesoscale modelling for the northern domain. The lower panels show the difference compared to the 'control' resolution of 5 km. Red contours indicate negative differences, blue contours positive differences. Contours increase in absolute value with increasing thickness, going from 1, 2, 4, 8, 16 %. Statistics for the differences in % are given above the difference maps.*

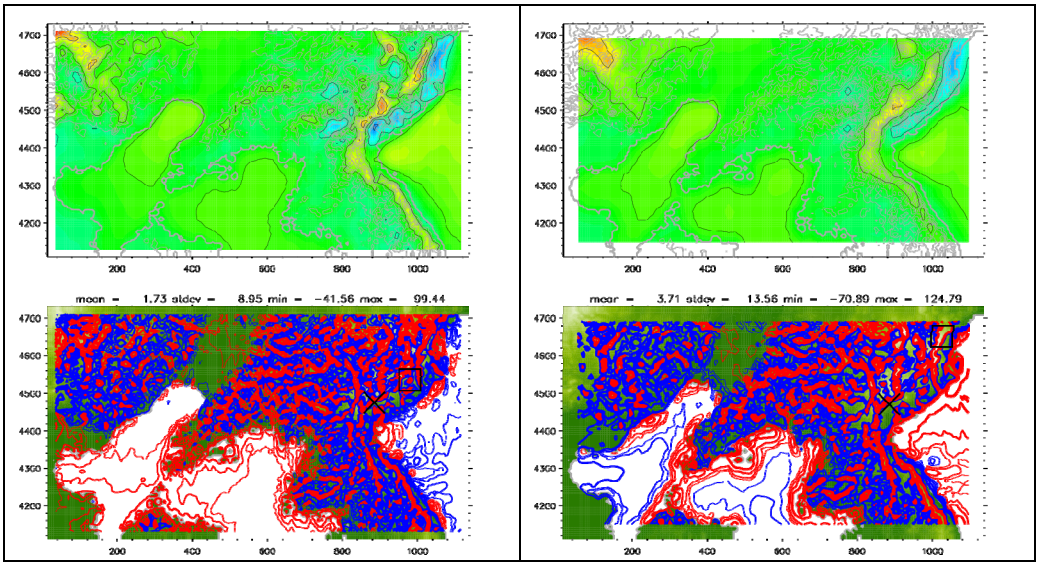


*Figure45: Maps of mean simulated wind speed at 100 m (upper panels) for 10 km (left) and 20 km (right) resolution mesoscale modelling for the northern domain. The lower panels show the difference compared to the 'control' resolution of 5 km. Red contours indicate negative differences, blue contours positive differences. Contours increase in absolute value with increasing thickness, going from 1, 2, 4, 8, 16 %. Statistics for the differences in % are given above the difference maps.*

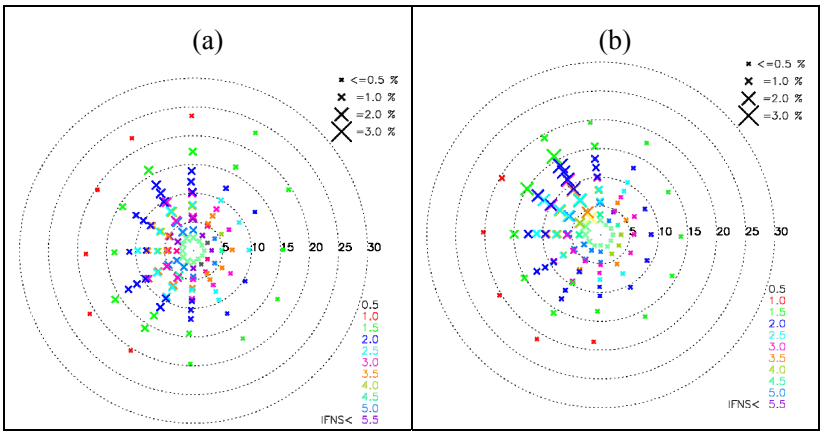


*Figure 46: (a) Wind class set 'NN_11' based on geostrophic winds at 0m at 131.25E 46.25N and (b) wind class set 'NN_20' based on geostrophic winds at 1500 m at 126.25E 48.75N, used for the northern domain.*

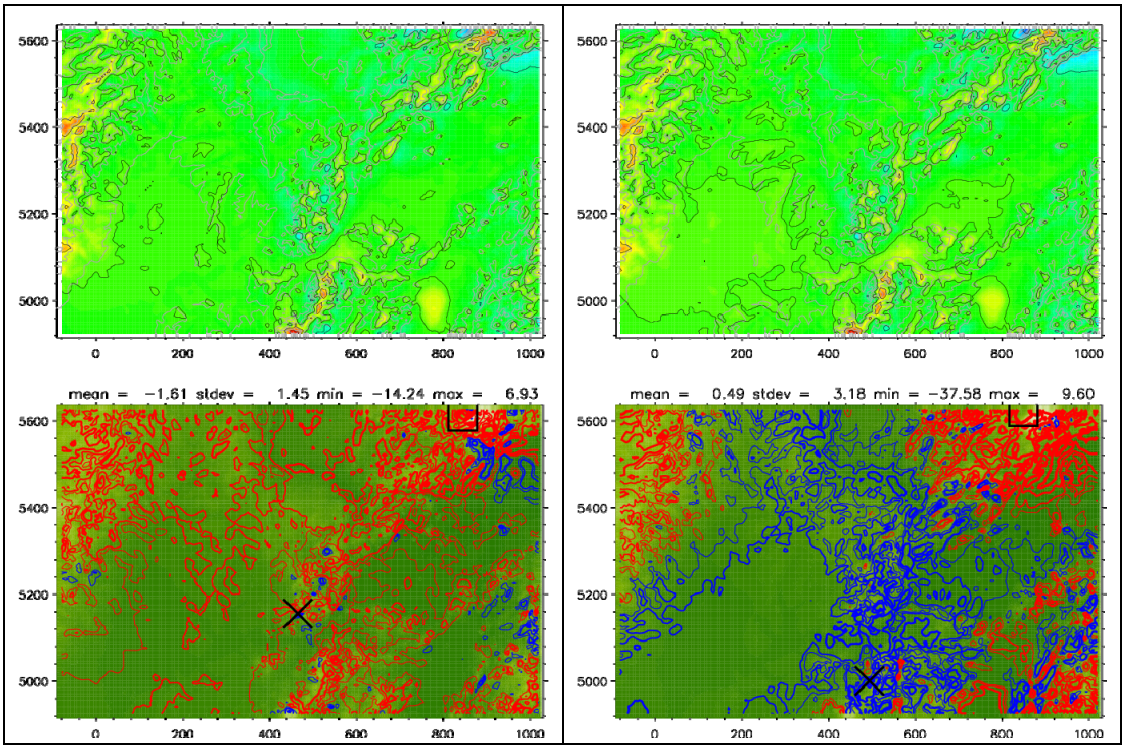


*Figure 47: Maps of mean simulated wind speed at 100 m (upper panels) using wind class set 'NN_11' defined at a different horizontal location (left) and wind class set 'NN_20' defined at a different vertical location (right) for the northern domain. The lower panels show the difference compared to the 'control' wind class set. Red contours indicate negative differences, blue contours positive differences. Contours increase in absolute value with increasing thickness, going from 1, 2, 4, 8, 16 %. Statistics for the differences in % are given above the difference maps.*

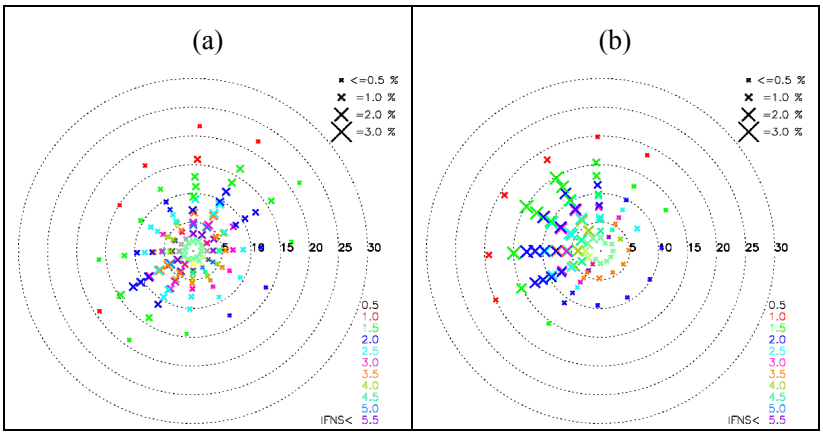


*Figure 48: (a) Wind class set 'NS_11' based on geostrophic winds at 0m at 121.25E 38.75N and (b) wind class set 'NS_20' based on geostrophic winds at 1500 m at 121.25E 41.25N, used for the southern domain.*

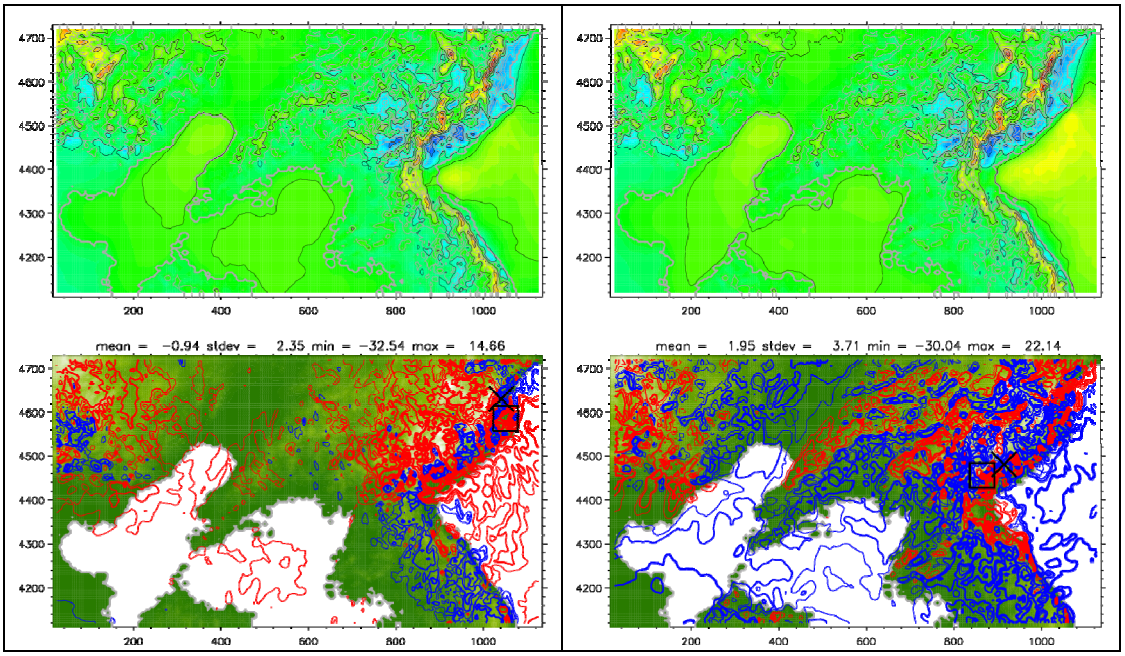


*Figure 49: Maps of mean simulated wind speed at 100 m (upper panels) using wind class set 'NS_11' defined at a different horizontal location (left) and wind class set 'NS_20' defined at a different vertical location (right) for the southern domain. The lower panels show the difference compared to the 'control' wind class set. Red contours indicate negative differences, blue contours positive differences. Contours increase in absolute value with increasing thickness, going from 1, 2, 4, 8, 16 %. Statistics for the differences in % are given above the difference maps.*

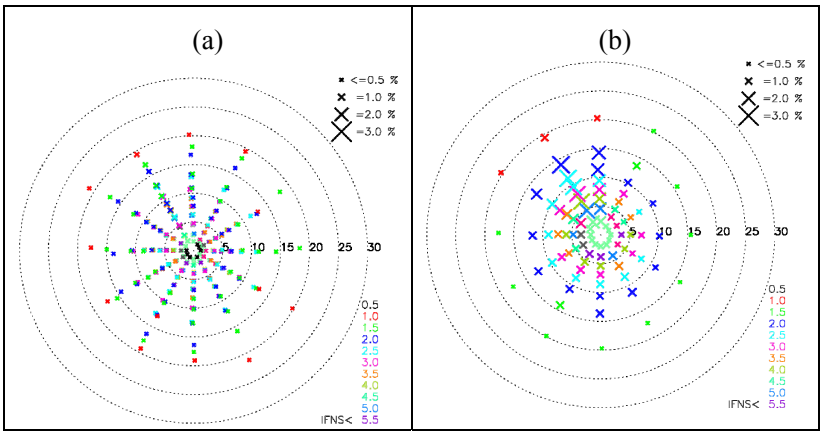


*Figure 50: (a) Wind class set 'NN_30' using 3 stability classes and (b) wind class set 'NN_40' based on 1 stability class, used for the centre domain.*

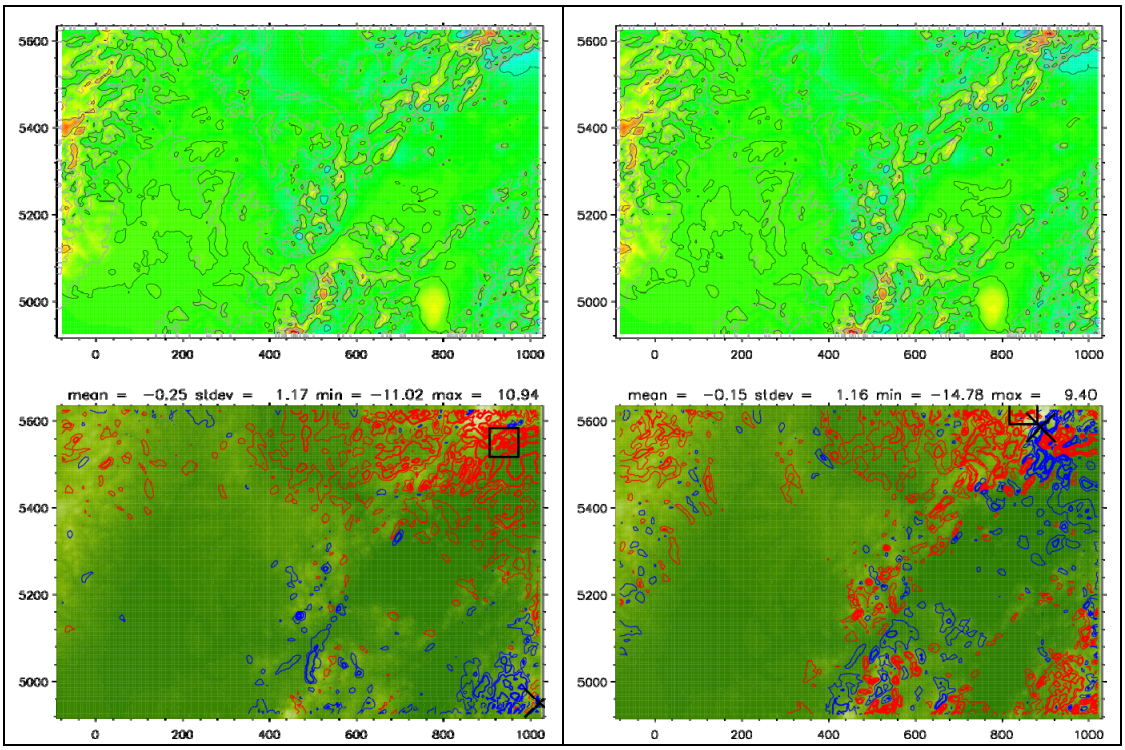


*Figure 51: Maps of mean simulated wind speed at 100 m (upper panels) using wind class set 'NN_30' based on 3 stability classes wind (left) and wind class set 'NN_40' based on 1 stability class (right) for the northern domain. The lower panels show the difference compared to the 'control' wind class set. Red contours indicate negative differences, blue contours positive differences. Contours increase in absolute value with increasing thickness, going from 1, 2, 4, 8, 16 %. Statistics for the differences in % are given above the difference maps.*

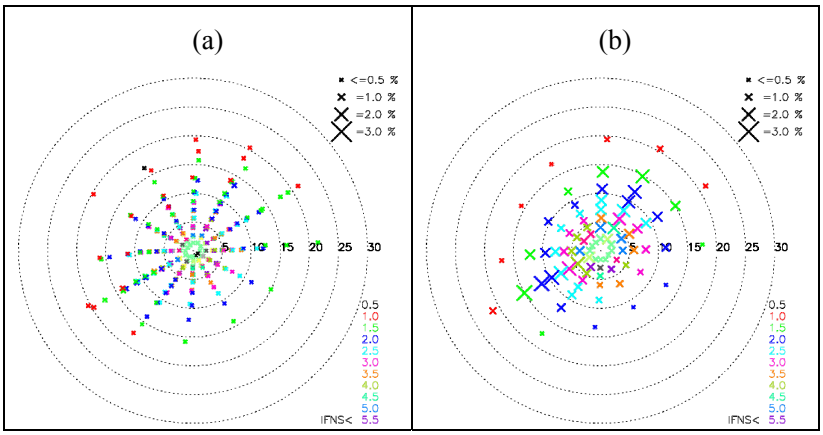


*Figure 52: (a) Wind class set 'NS_30' using 3 stability classes and (b) wind class set 'NS_40' based on 1 stability class, used for the centre domain.*

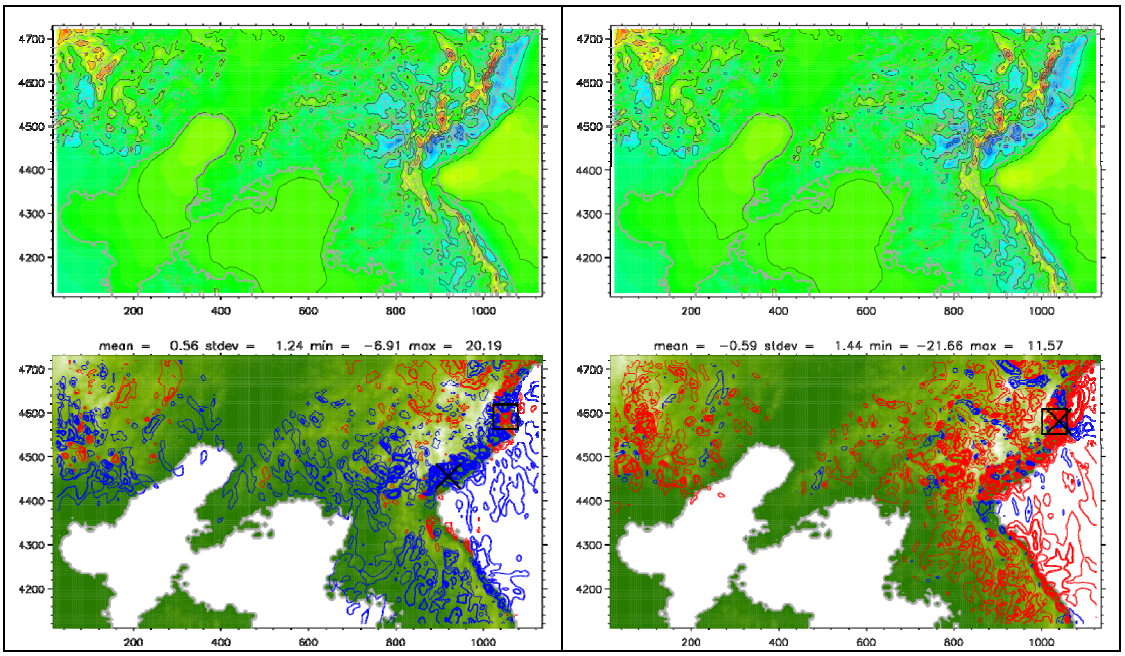


*Figure 53: Maps of mean simulated wind speed at 100 m (upper panels) using wind class set 'NS_30' based on 3 stability classes wind (left) and wind class set 'NS_40' based on 1 stability class (right) for the northern domain. The lower panels show the difference compared to the 'control' wind class set. Red contours indicate negative differences, blue contours positive differences. Contours increase in absolute value with increasing thickness, going from 1, 2, 4, 8, 16 %. Statistics for the differences in % are given above the difference maps.*

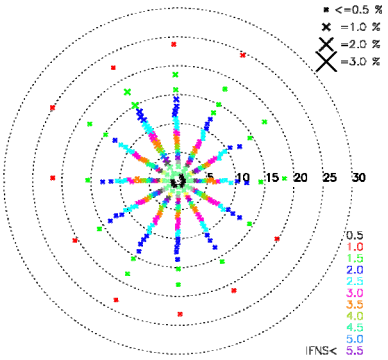


*Figure 54: Wind class set 'NN_50' using 1 stability class, used for the northern domain.*

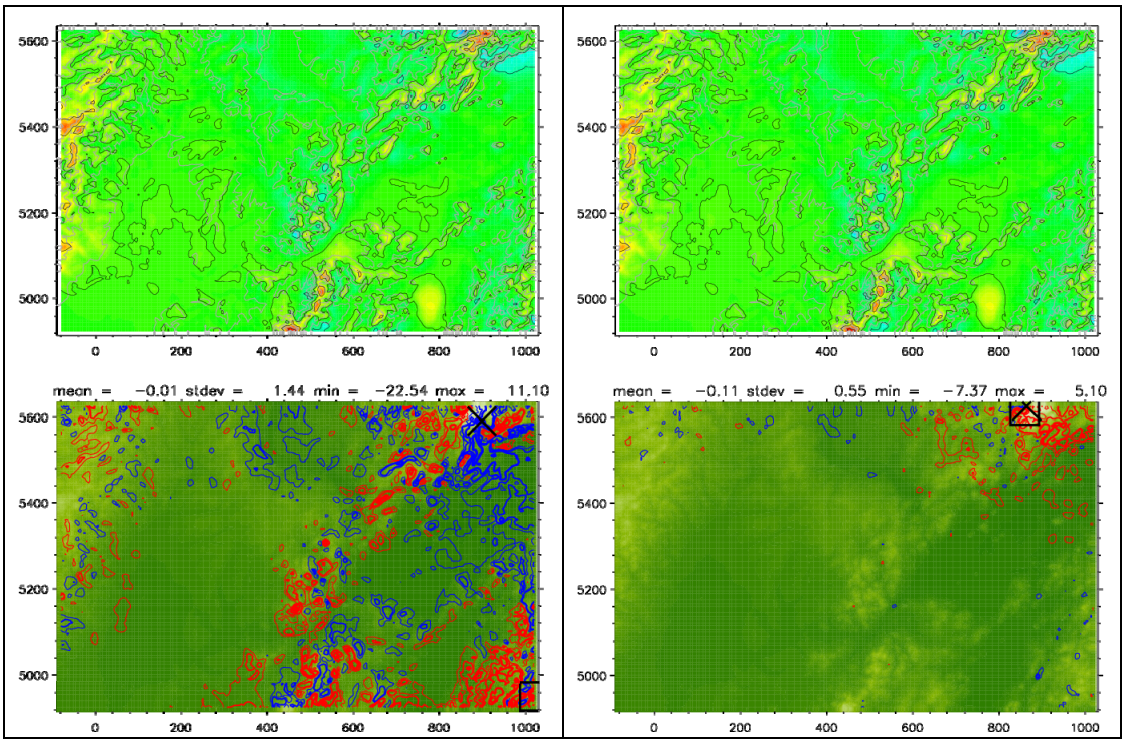


*Figure 55: Maps of mean simulated wind speed at 100 m (upper panels) using wind class set 'NN_50' based on 1 stability class wind (left and right) for the northern domain. The lower panels show the difference compared to a wind class set 'NN_30' based on 3 stability classes (left) and compared to a wind class set 'NN_40' based on 1 stability class but reduced number of wind classes. Red contours indicate negative differences, blue contours positive differences. Contours increase in absolute value with increasing thickness, going from 1, 2, 4, 8, 16 %. Statistics for the differences in % are given above the difference maps.*

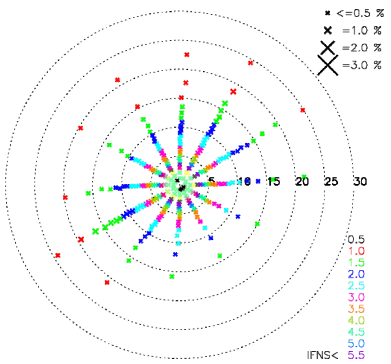


*Figure 56: Wind class set 'NS_50' using 1 stability class, used for the southern domain.*

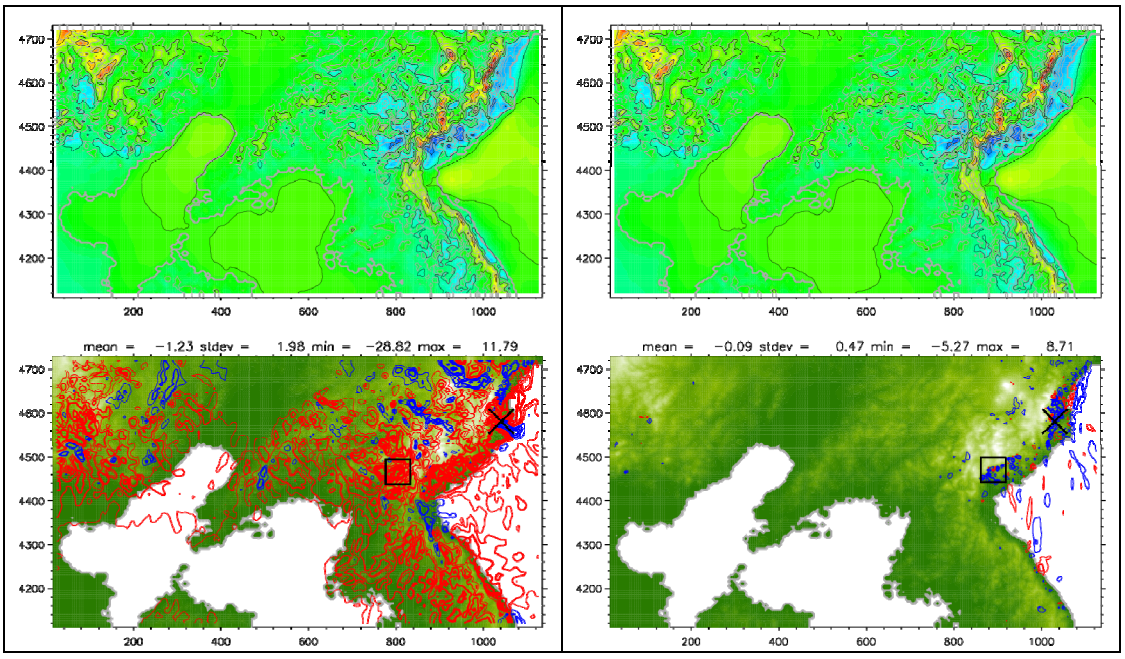


*Figure 57: Maps of mean simulated wind speed at 100 m (upper panels) using wind class set 'NS_50' based on 1 stability class wind (left and right) for the southern domain. The lower panels show the difference compared to a wind class set 'NS_30' based on 3 stability classes (left) and compared to a wind class set 'NS_40' based on 1 stability class but reduced number of wind classes. Red contours indicate negative differences, blue contours positive differences. Contours increase in absolute value with increasing thickness, going from 1, 2, 4, 8, 16 %. Statistics for the differences in % are given above the difference maps.*

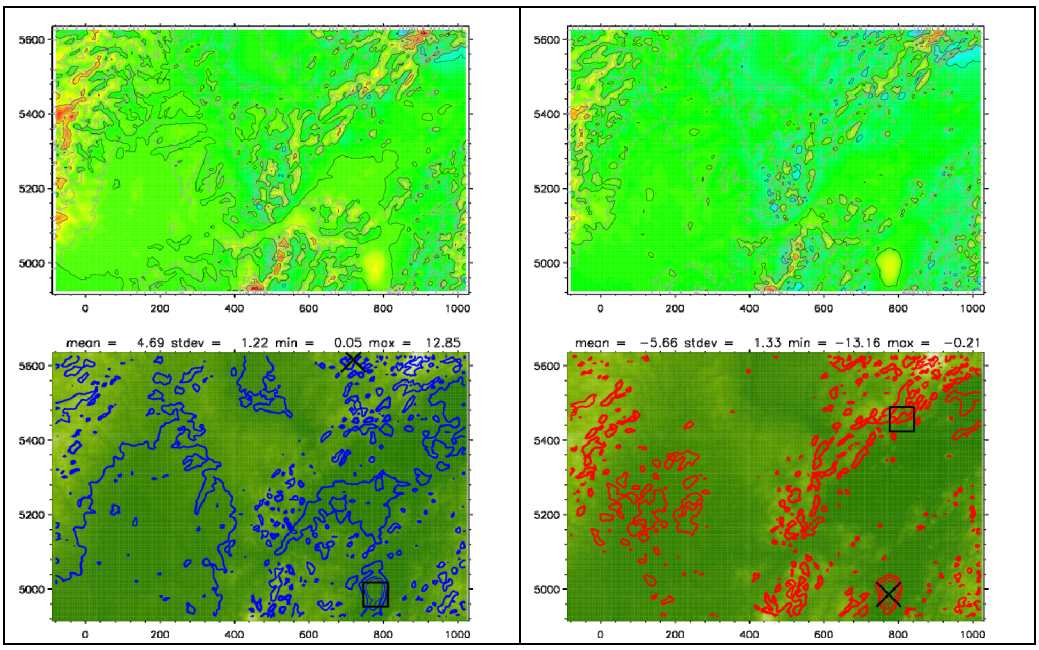


*Figure 58: Maps of mean simulated wind speed at 100 m (upper panels) where land roughness lengths are halved (left) and where land roughness lengths are doubled (right) for the northern domain. The lower panels show the difference compared to the 'control' using nominal roughness lengths.*

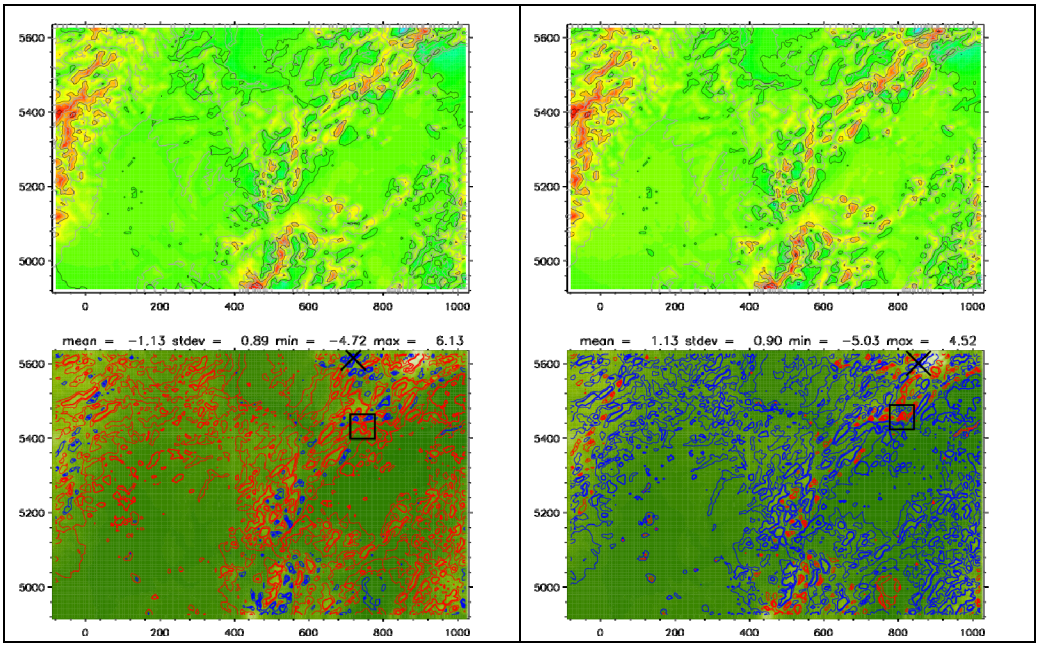


*Figure 59: Maps of generalized wind speed at 100 m (upper panels) where land roughness lengths are halved (left) and where land roughness lengths are doubled (right) for the northern domain. The lower panels show the difference compared to the 'control' using nominal roughness lengths. Red contours indicate negative differences, blue contours positive differences. Contours increase in absolute value with increasing thickness, going from 1, 2, 4, 8, 16 %. Statistics for the differences in % are given above the difference maps.*

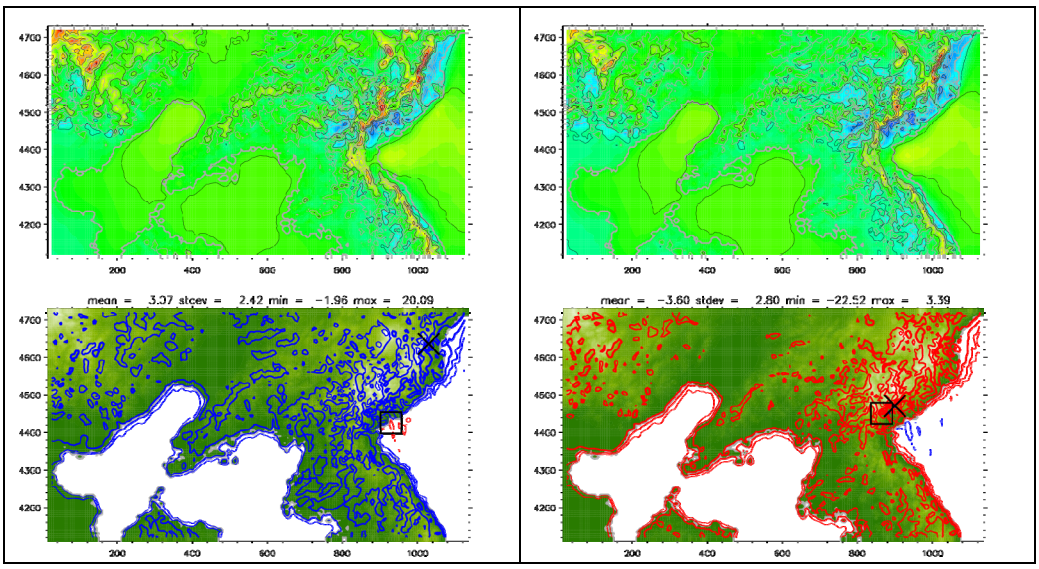


*Figure 60: Maps of mean simulated wind speed at 100 m (upper panels) where land roughness lengths are halved (left) and where land roughness lengths are doubled (right) for the southern domain. The lower panels show the difference compared to the 'control' using nominal roughness lengths.*

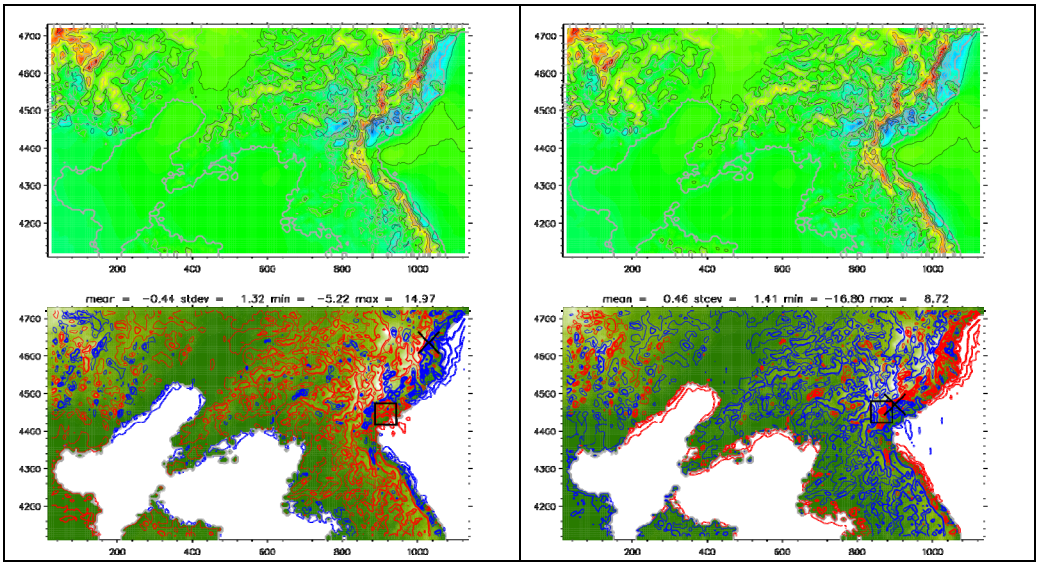


*Figure 61: Maps of generalized wind speed at 100 m (upper panels) where land roughness lengths are halved (left) and where land roughness lengths are doubled (right) for the southern domain. The lower panels show the difference compared to the 'control' using nominal roughness lengths. Red contours indicate negative differences, blue contours positive differences. Contours increase in absolute value with increasing thickness, going from 1, 2, 4, 8, 16 %. Statistics for the differences in % are given above the difference maps.*

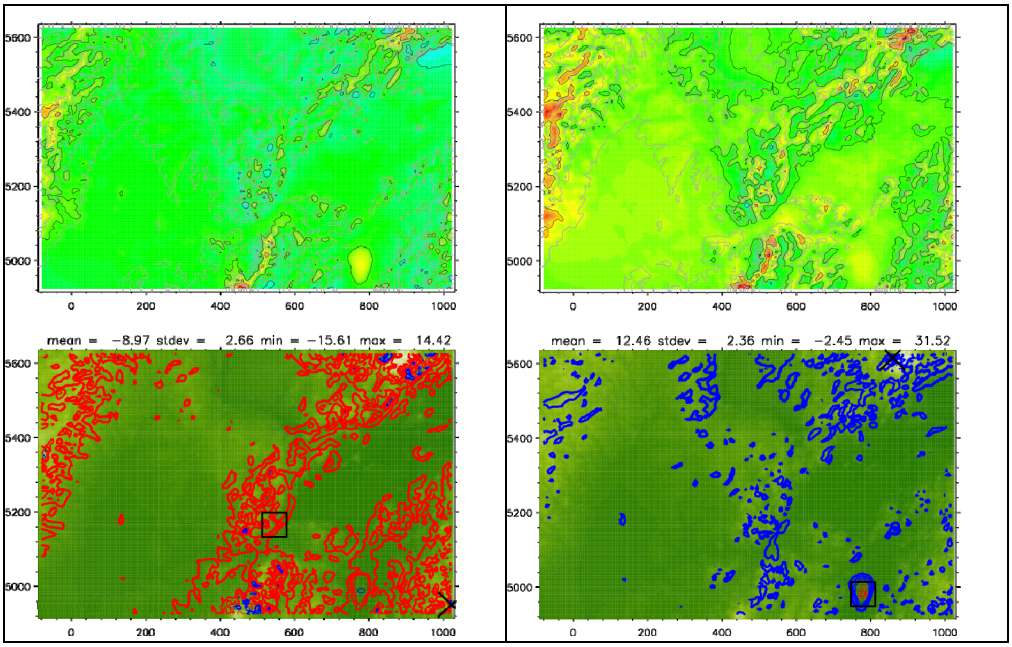


*Figure 62: Maps of mean simulated wind speed at 100 m (upper panels) for warm-land / cool-sea configuration (left) and for cool-land / warm-sea configuration (right) for the northern domain. The lower panels show the difference compared to the 'control' configuration with surface surface-air temperature equilibrium at initial time. Red contours indicate negative differences, blue contours positive differences. Contours increase in absolute value with increasing thickness, going from 1, 2, 4, 8, 16 %. Statistics for the differences in % are given above the difference maps.*

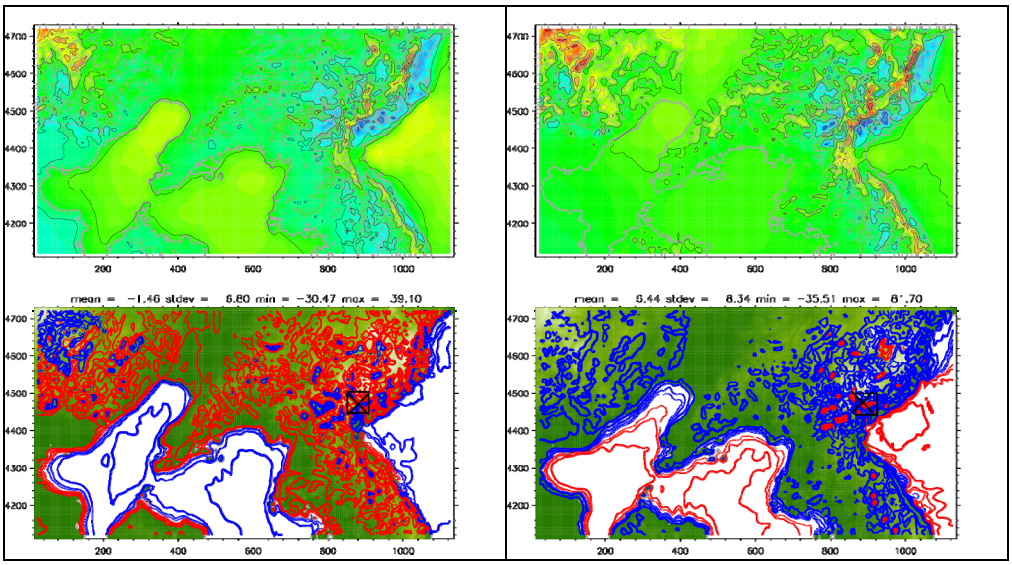


*Figure 63: Maps of mean simulated wind speed at 100 m (upper panels) for warm-land / cool-sea configuration (left) and for cool-land/warm-sea configuration (right) for the southern domain. The lower panels show the difference compared to the 'control' configuration with surface surface-air temperature equilibrium at initial time. Red contours indicate negative differences, blue contours positive differences. Contours increase in absolute value with increasing thickness, going from 1, 2, 4, 8, 16 %. Statistics for the differences in % are given above the difference maps.*

# 20 Appendix B – associated data files

**WAsP lib-file dataset**

The lib-files (.lib file extension) are named according to location using the following convention; *DDb05_10_eee.eee*E_*nn.nnn*N_7.4_5.lib, where *DD* is the domain from which the data comes, and *eee.eee* and *nn.nnn* are the longitude and latitude in decimal degrees respectively.

DD can have values of NN; NC, and NS, corresponding to the northern, centre, and southern domains respectively.

For locations north of 46$^{o}$N, the northern domain should be used (DD = NN).

For locations south of 46$^{o}$N and north of 42$^{o}$N, the centre domains should be used (DD=NC).

For locations south of 42$^{o}$N, the southern domain should be used (DD = NS).

The files are available in the form of zipped files for each domain:

NN_LibGrid.zip containing 18360 lib-files

NC_LibGrid.zip containing 15660 lib-files

NS_LibGrid.zip containing 15660 lib-files

**Map grd-files dataset**

Surfer grid files (.grd file extension) are given for the entire region of interest for the wind resource maps (wind speed and power density ) at 50, 70, and 100 m and generalized wind climate (wind speed and power density) for 0.03 m roughness flat terrain at 50, 70 and 100 m.

The files are zipped in to files pertaining to the three heights.

NEChinaNNb05_10_z50.zip

NEChinaNNb05_10_z70.zip

NEChinaNNb05_10_z100.zip

The files use longitude and latitude (datum WGS84) as the coordinate system. Wind speeds are given in m/s and power density in W/m$^2$.

The file naming convention is:

NEChinaNNb05_10_zHHH.5.TTT.F_i_merge.grd

Where HHH is the height (50, 70, or 100 m), TTT is the data type (wrm = wind resource map, i.e. simulated wind climate, or wam = wind atlas map, i.e. generalized wind climate), and F is the field (u = wind speed or e = power density).

[Start the report here - Do not delete the following line since it contains a Section Break]

Risø DTU is the National Laboratory for Sustainable Energy. Our research focuses on development of energy technologies and systems with minimal effect on climate, and contributes to innovation, education and policy. Risø has large experimental facilities and interdisciplinary research environments, and includes the national centre for nuclear technologies.

**Risø DTU**
**National Laboratory for Sustainable Energy**
**Technical University of Denmark**

Frederiksborgvej 399
PO Box 49
DK-4000 Roskilde
Denmark
Phone +45 4677 4677
Fax +45 4677 5688

www.risoe.dtu.dk